NASA TECHNICAL MEMORANDUM

NASA TM X-2311

NASA TM X-2311

CALCULATION OF CAMBER USING SLENDER WING THEORY AT MACH NUMBER 1.0

by William B. Igoe

Langley Research Center

Hampton, Va. 23365

NATIONAL AERONAUTICS AND SPACE ADMINISTRATION • WASHINGTON, D. C. • SEPTEMBER 1971

1. Report No.	2. Government Accession No.	3. Recipient's Catalog No.
NASA TM X-2311		

4. Title and Subtitle	5. Report Date
CALCULATION OF CAMBER USING SLENDER WING THEORY AT MACH NUMBER 1.0	September 1971
	6. Performing Organization Code
7. Author(s)	8. Performing Organization Report No.
William B. Igoe	L-7666
	10. Work Unit No.
9. Performing Organization Name and Address	136-13-01
NASA Langley Research Center Hampton, Va. 23365	11. Contract or Grant No.
	13. Type of Report and Period Covered
12. Sponsoring Agency Name and Address	Technical Memorandum
National Aeronautics and Space Administration Washington, D.C. 20546	14. Sponsoring Agency Code

15. Supplementary Notes

The information presented herein is based on a thesis submitted in partial fulfillment of the requirements for the degree of Master of Science in Aeronautical Engineering, George Washington University, Washington, D.C., February 1971.

16. Abstract

A calculation procedure based on slender wing theory at Mach number 1.0 is presented for the determination of the mean line camber ordinates for laterally symmetrical wings with polygonal planforms. A uniform chordwise load and a continuous but otherwise arbitrary spanwise load distribution is assumed. The procedure is generally limited to slender wings at high subsonic speeds and low lift coefficients.

Graphs of functions required in the calculation procedure are presented. In addition, an application of the method of calculation for a variable-sweep wing planform is described and some calculated camber results are shown. Although the slender wing theory for Mach number 1.0 is considered to be inadequate for the calculation of the detailed shape of airfoil section camber for supercritical wings designed for near-sonic speeds, a comparison with experimental results shows that it predicts the general magnitude and trend of the spanwise variation of the wing twist angle.

17. Key Words (Suggested by Author(s))	18. Distribution Statement
Slender wing theory Wing camber Supercritical wing	Unclassified – Unlimited

19. Security Classif. (of this report)	20. Security Classif. (of this page)	21. No. of Pages	22. Price*
Unclassified	Unclassified	72	$3.00

*For sale by the National Technical Information Service, Springfield, Virginia 22151

CALCULATION OF CAMBER USING SLENDER WING THEORY AT MACH NUMBER 1.0*

By William B. Igoe
Langley Research Center

SUMMARY

A calculation procedure based on slender wing theory at Mach number 1.0 is presented for the determination of the mean line camber ordinates for laterally symmetrical wings with polygonal planforms. A uniform chordwise load and a continuous but otherwise arbitrary spanwise load distribution is assumed. The procedure is generally limited to slender wings at high subsonic speeds and low lift coefficients.

Graphs of functions required in the calculation procedure are presented. In addition, an application of the method of calculation for a variable-sweep wing planform is described and some calculated camber results are shown. Although the slender wing theory for Mach number 1.0 is considered to be inadequate for the calculation of the detailed shape of airfoil section camber for supercritical wings designed for near-sonic speeds, a comparison with experimental results shows that it predicts the general magnitude and trend of the spanwise variation of the wing twist angle.

INTRODUCTION

Slender wing theory was introduced in 1946 by Robert T. Jones in reference 1, and in 1948, the application to sonic flow was stated explicitly by Heaslet, Lomax, and Spreiter in reference 2. At about the same time, similar results were obtained in England by A. Robinson and in France by R. Legendre, E. A. Eichelbrenner, and A. von Baranoff. Detailed references to these developments are contained in volumes 6 and 7 of the Princeton Series on High Speed Aerodynamics and Jet Propulsion. (See refs. 3 and 4.)

As shown in reference 2, the linearized potential flow theory equation relating the downwash of a slender lifting wing to its load has an especially simple form at Mach 1. This equation for the downwash at a field point on a wing at Mach 1 has the same form as the incompressible flow equation for the downwash in the far wake (neglecting rollup of the

---

*The information presented herein is based on a thesis submitted in partial fulfillment of the requirements for the degree of Master of Science in Aeronautical Engineering, George Washington University, Washington, D.C., February 1971.

trailing-vortex sheet) downstream of the field point for that part of the wing ahead of the field point. The relationship between the sonic and incompressible flow fields is easily visualized when the Prandtl-Glauert compressibility factor for Mach 1 is considered as stretching the wing dimensions infinitely in the streamwise direction. The pressure signals in the zone of silence behind a sonic Mach line through the field point cannot propagate upstream in sonic flow. Therefore, only that part of the wing forward of the field point contributes to the downwash at the field point.

The simple form of the downwash equation for a slender lifting wing in sonic flow and its resemblance to the far-wake downwash equation of incompressible flow allows a simple solution to be used. This solution is similar to the lifting-line theory solution of Glauert in reference 5 for incompressible flow. By following Glauert's method, the sonic wing downwash velocity, and thereby the local streamwise slope of the wing-section cambered mean lines, may be expressed in terms of the coefficients of a Fourier sine series. This series represents the partial spanwise load distribution of that part of the wing ahead of the field point. The local cambered mean line slopes may then be integrated streamwise to obtain cambered mean line ordinates.

For the special case of a polygonal wing planform with lateral symmetry and with uniform chordwise load, the Fourier coefficients for computing cambered mean line slopes and similar coefficients for computing cambered mean line ordinates have been derived for continuous but otherwise arbitrary spanwise load distributions. The sum of the resulting series expression for cambered mean line ordinates has been taken to obtain a closed-form solution. This closed-form solution avoids the necessity of evaluating a term-by-term summation of a slowly convergent series which requires a large number of terms for numerical accuracy. The resulting solution is applicable to a variety of wing planforms, including those typical of variable-sweep wings. It can be extended to other planforms by means of superposition. Ths usefulness of the slender wing theory at Mach 1 is mainly for wings at high subsonic speeds. As indicated in reference 2, this simplified form of the linear theory should be applicable for wings for which the slenderness parameter βA is small.

Graphs of the functions encountered in the closed-form solution are presented and an application of the method of calculation for a variable-sweep wing planform is described. Some calculated camber results are included and the theoretical wing twist distribution for a supercritical wing designed for near-sonic speeds is compared with an experimentally obtained twist distribution.

SYMBOLS

A	aspect ratio
A_m	coefficient in trigonometric sine series representing the wing-section design lift coefficient distribution (see eq. (A4))
B_n	coefficient in Fourier sine series representing the partial wing spanwise load distribution (see eq. (4))
b	wing span
C_L	wing lift coefficient
C_n	coefficient in series solution for wing mean line camber ordinates (see eq. (8))
C_p	pressure coefficient
$\Delta C_p = (C_p)_{\text{lower surface}} - (C_p)_{\text{upper surface}}$	
c	wing chord $\left(\text{streamwise, in general, except for } c_t \text{ with } \sigma < \frac{\pi}{2}\right)$
c_{av}	average chord, S/b
c_l	section lift coefficient
D_m	function in analytical summation of series (see eq. (C1))
d_1	perpendicular distance from wing pivot point to wing leading edge
d_2	perpendicular distance from wing pivot point to wing trailing edge
d_3	perpendicular distance from wing pivot point to wing-tip chord
E_m	function in analytical summation of series (see eq. (C4))
F,G,H,I	functions of n, m, and θ (see eqs. (A11), (A12), (B6), and (B7))

K_m function in recursion formula solution for A_m coefficients for elliptical spanwise load distribution on straight-tapered wings (see eq. (E5))

$k = \tan \Lambda$ (with exception of $k_3 = -\tan \sigma$)

$k' = \tan \Lambda'$ (with exception of $k_3' = -\tan \sigma'$)

$L_{m,s}$ functions in summation for wing mean line camber ordinate (see eq. (14))

l length of variable-sweep wing in fully swept position with straight leading edge (before truncation)

M free-stream Mach number

m index in trigonometric series for section lift coefficient distribution (odd integers only for wings with lateral symmetry)

n index in Fourier series for P^* (odd integers only for wings with lateral symmetry)

P^* partial wing spanwise load distribution function (see eq. (2))

p integer

r index of summation

S wing area

S^* partial wing area

s index of summation of $L_{m,s}$ functions (see eq. (14))

V free-stream velocity (parallel to X-axis)

w downwash velocity (parallel to Z-axis)

x,y,z streamwise, spanwise, and vertical orthogonal Cartesian coordinates with origin at the wing leading-edge apex

x_a streamwise distance from leading-edge apex to intersection with X-axis of line projected from outboard leading edge of variable-sweep wing panel

x_b streamwise distance from leading-edge apex to intersection with X-axis of line projected from wing tip chord $\left(\text{for } \sigma < \frac{\pi}{2}\right)$

x_{le} streamwise location of leading edge of local chord

Δx_0 local streamwise distance from wing leading edge to field point

y_l span of variable-sweep wing in fully swept position (before truncation)

y_1 spanwise point at which Mach line (x_0 = Constant) through field point intersects the wing leading edge

y_2 spanwise point at which Mach line (x_0 = Constant) through field point intersects the wing trailing edge

y_3 spanwise point at which the Mach line (x_0 = Constant) through field point intersects the inward slanted wing tip $\left(\text{for } \sigma < \frac{\pi}{2}\right)$

Δz_0 camber ordinate measured with respect to leading edge of local streamwise chord $\left(\Delta z_0 = z_0 - z_{le}\right)$

$\beta = (1 - M^2)^{1/2}$

Δ difference

δ angle between wing outboard leading and trailing edges $\left(\delta = \Lambda_1 - \Lambda_2\right)$

ϵ wing twist angle

$\theta = \cos^{-1}(-y)$

Λ sweep angle

λ taper ratio for straight-tapered wings

σ angle of wing tip chord with respect to Mach line $\left(\sigma = \sigma' + \Lambda_1' - \Lambda_1\right)$

Subscripts:

A,B	lower and upper limits. x_A corresponds to wing leading edge and x_B corresponds to wing trailing edge or line x_0 in general. y_A and y_B correspond to left and right wing tips or to $-y_1$ and y_1, respectively. θ_A and θ_B are similarly defined
k	wing leading-edge kink for variable-sweep wings
le	leading edge
p	wing pivot
r	wing root
te	trailing edge
t	wing tip
0	field point
1	wing leading edge
2	wing trailing edge
3	wing tip

Superior or overhead bar ($\bar{}$) indicates dimensional length. Unbarred lengths are nondimensionalized with respect to the wing semispan. Asterisk (*) superscript indicates partial wing parameter. Prime (') superscript indicates wing geometric characteristics when leading edge is straight for variable-sweep wing.

BASIC EQUATIONS

In linearized wing theory, the equation relating the downwash or normal induced velocity at a field point to the partial loading ahead of the field point for a slender lifting wing at $M = 1$ is given by equation (62) of reference 2. This equation may be written as

$$\frac{w_0}{V} = -\frac{1}{4\pi}\int_{y_A}^{y_B} \frac{\frac{\partial P^*}{\partial y}}{y_0 - y}\,dy \tag{1}$$

where

$$P^* = \int_{x_A}^{x_B} \Delta C_p \, dx \tag{2}$$

and the limits of integration are established by the boundaries of the region S^* as shown in figure 1. Satisfaction of the Kutta condition at the wing trailing edge is assured by imposing the condition that the load distribution is zero behind the trailing edge. The velocity ratio in equation (1) is equal to twice the normal induced velocity ratio in the near wake for incompressible flow (see ref. 5, for example) for a lifting-line wing consisting only of the region S^*. The factor of two accounts for the difference between near-wake and far-wake conditions if rollup of the wing trailing vortex sheet is neglected.

A well-known method of evaluating the improper integral of equation (1) with the use of Fourier analysis was shown by Glauert (ref. 5). By following reference 5, the spanwise variable θ is introduced so that

$$y = -\cos \theta \tag{3}$$

where θ varies from 0 to π as y varies from -1 to 1 as shown in figure 2. The partial load function P^* is then expanded in a Fourier series

$$P^* = \sum_{n=1}^{\infty} B_n \sin n\theta \tag{4}$$

With the use of equations (3) and (4), the integral of equation (1) becomes

$$\frac{w_0}{V} = -\frac{1}{4\pi} \int_{\theta_A}^{\theta_B} \frac{\sum_{n=1}^{\infty} nB_n \cos n\theta}{\cos \theta - \cos \theta_0} \, d\theta \tag{5}$$

The order of summation and differentiation has been interchanged in obtaining equation (5). Reference 6 shows that this interchange of order is permissible if the function P^* is continuous and if its derivative is sectionally continuous in the interval $-\pi \leqq \theta \leqq \pi$. In general, this requirement is satisfied for wings with span load distributions which are everywhere continuous. The conditions on P^* are also sufficient to permit the interchange of order of summation and integration. Accordingly, the integral of equation (5) may be taken inside the summation sign and evaluated as shown in reference 5 to obtain

$$\frac{w_0}{V} = -\frac{1}{4} \sum_{n=1}^{\infty} \frac{nB_n \sin n\theta_0}{\sin \theta_0} \tag{6}$$

In this step the lower and upper limits of integration for θ have been taken as 0 and π, respectively. The extension of the limits for θ beyond those defined by S* is possible if the function P* is defined as being zero outside the region S*.

The slope of the mean line camber is equal to the downwash velocity ratio

$$\frac{dz}{dx} = \frac{w}{V}$$

Hence the slope of the mean line camber may be obtained directly from equation (6). Integration of equation (6) with respect to x gives the mean line camber ordinate

$$z = -\frac{1}{4 \sin \theta_0} \sum_{n=1}^{\infty} nC_n \sin n\theta_0 \tag{7}$$

where

$$C_n = \int_0^{x_0} B_n \, dx \tag{8}$$

and again the order of summation and integration has been interchanged. By taking the integral limits on x from 0 to the field point x_0, the camber ordinates are obtained with respect to the leading-edge apex. An indeterminate form is encountered in equations (6) and (7) for field points at the wing tip where $\theta_0 = \pi$. The limiting form is seen to be

$$\lim_{\theta \to \pi} \frac{\sin n\theta}{\sin \theta} = n(-1)^{n+1}$$

Thus, for $\theta_0 = \pi$, equations (6) and (7) may be rewritten as

$$\frac{w_0}{V} = -\frac{1}{4} \sum_{n=1}^{\infty} n^2 B_n (-1)^{n+1} \qquad (\theta_0 = \pi) \tag{9}$$

and

$$z = -\frac{1}{4} \sum_{n=1}^{\infty} n^2 C_n (-1)^{n+1} \qquad (\theta_0 = \pi) \tag{10}$$

The series summations of equations (9) and (10) are generally not convergent so that $\frac{w_0}{V} \to \infty$ and $z \to \infty$ as $\theta_0 \to \pi$. Equations (6) and (7) have not been restricted as to wing planform or load distribution with the exception that the partial load function P* must be continuous and have a sectionally continuous first derivative. In the following analysis, the applications are restricted to wings with lateral symmetry and with a uniform

chordwise load distribution. This chordwise load distribution causes infinite camber slopes to appear at the leading and trailing edges but the camber ordinates are finite except at the discontinuities represented by the wing root, wing tip, and wing leading-edge sweep discontinuity in the case of a variable-sweep wing.

For a uniform chordwise load distribution, the B_n Fourier coefficients of equation (4) are evaluated in appendix A for a wing planform and a field-point location similar to that shown in figure 2. For the same conditions, an evaluation of the C_n coefficients of equation (8) is shown in appendix B. The results of an analytical summation of the series of equation (7) are presented in appendix C and an example of the procedure used in obtaining the summation terms is shown in appendix D. Some methods of obtaining the A_m coefficients which are needed to define the spanwise section lift coefficient distribution

$$c_l = \sum_m A_m \sin m\theta \tag{11}$$

are discussed in appendix E.

The application of the method of calculating camber is shown for wings with less restricted planform geometry and field-point location than are considered in appendixes A and B. However, the limitation of uniform chordwise load distribution is retained.

APPLICATION TO WINGS OF SPECIFIED PLANFORM

The equations developed in the preceding section and in appendixes A, B, and C are extended and applied to a wing planform with discontinuous slope (sweep angle) of the leading edge. This planform configuration is encountered in variable-sweep wings of the type shown in figure 3. The leading edges are idealized as straight continuous line segments. The trailing edges are taken as continuous straight lines with continuous sweep angles. Wings with swept forward leading or trailing edges or with wing tips that are leading edges are not considered. The leading-edge sweep of the outboard portion of the wing is limited to angles equal to or less than the leading-edge sweep of the fixed inboard part of the wing. The latter conditions may be expressed as

$$0 \leqq \Lambda_1 \leqq \Lambda_1'$$

$$0 \leqq \Lambda_2 \leqq \Lambda_1' - \delta$$

$$0 \leqq \sigma \leqq \frac{\pi}{2}$$

Although other planform configurations are possible in variable-sweep wings, the configurations included under these conditions are considered the ones most likely to be encountered in practice.

Wing Geometry

The equations in the preceding section and in appendixes A, B, and C have been developed for a wing of unit semispan. However, for variable-sweep wings the geometry, including the semispan, changes with sweep angle. It will be convenient in the camber calculations to consider certain geometrical parameters describing the variable-sweep planforms to be dimensional in character. The wing geometry will then be nondimensionalized in terms of the semispan for each wing-sweep angle. The dimensional parameters will be indicated by a superior or overhead bar. Plain or unbarred parameters will be nondimensional. The following fixed constants will be considered given: Λ_1', δ, σ', $\bar{x}_p$, $\bar{y}_p$, $\bar{d}_3$, $\bar{c}_t$, and $\bar{c}_r'$. In addition, the variable-sweep angle Λ_1 of the leading edge of the outboard part of the wing will also be given.

The quantities which are needed to introduce the effects of variable-wing geometry into the wing camber calculations can be computed from the input constants and Λ_1. The physical significance of most of the following geometrical quantities can be inferred from the sketch of figure 3. The first step is to obtain the angles and slopes of the various edges of the wing under variable-sweep conditions:

$$\Lambda_2 = \Lambda_1 - \delta$$

$$\Lambda_2' = \Lambda_1' - \delta$$

$$\sigma = \sigma' + \Lambda_1' - \Lambda_1$$

$$k_1 = \tan \Lambda_1$$

$$k_1' = \tan \Lambda_1'$$

$$k_2 = \tan \Lambda_2$$

$$k_2' = \tan \Lambda_2'$$

$$k_3 = -\tan \sigma$$

$$k_3' = -\tan \sigma'$$

The next step is to obtain the length parameters which are needed to establish the nondimensional geometry and the criteria for determining field-point regions under variable-sweep conditions:

$$\bar{d}_1 = \left(\bar{x}_p - k_1'\bar{y}_p\right)\cos\Lambda_1'$$

$$\frac{\bar{b}}{2} = \bar{y}_p + \frac{1}{k_1 - k_3}\left(\frac{\bar{d}_3}{\cos\sigma} + \frac{\bar{d}_1}{\cos\Lambda_1}\right) \qquad \left(\sigma' \leq \sigma < \frac{\pi}{2}\right)$$

$$\frac{\bar{b}}{2} = \bar{y}_p + \bar{d}_3 \qquad \left(\sigma = \frac{\pi}{2}\right)$$

$$\frac{\bar{b}'}{2} = \bar{y}_p + \frac{1}{k_1' - k_3'}\left(\frac{\bar{d}_3}{\cos\sigma'} + \frac{\bar{d}_1}{\cos\Lambda_1'}\right)$$

$$\bar{x}_a = \bar{x}_p - \frac{\bar{d}_1}{\cos\Lambda_1} - k_1\bar{y}_p$$

$$\bar{x}_b = \bar{x}_p + \frac{\bar{d}_3}{\cos\sigma} + \bar{y}_p\tan\sigma \qquad \left(\sigma' \leq \sigma < \frac{\pi}{2}\right)$$

$$\bar{d}_2 = \left(\bar{c}_r' + k_2'\bar{y}_p - \bar{x}_p\right)\cos\Lambda_2'$$

$$\bar{c}_r = \bar{x}_p + \frac{\bar{d}_2}{\cos\Lambda_2} - k_2\bar{y}_p$$

$$\bar{y}_k = \frac{\bar{x}_a}{k_1' - k_1} \qquad \left(\Lambda_1 < \Lambda_1'\right)$$

$$\bar{y}_k = \cos^2\Lambda_1'\left(k_1'\bar{x}_p + \bar{y}_p\right) \qquad \left(\Lambda_1 = \Lambda_1'\right)$$

$$\bar{x}_k = k_1'\bar{y}_k$$

The computed quantities Λ_2', k_1', k_2', k_3', $\bar{d}_1$, $\bar{d}_2$, $\bar{b}'/2$ do not change with the variable-sweep angle. The remainder of the quantities are functions of the sweep angle. The quantities $\bar{x}_a$, $\bar{x}_b$, $\bar{c}_r$, $\bar{y}_k$, and $\bar{x}_k$ are divided by the semispan $\bar{b}/2$ to obtain the nondimensionalized values of these quantities. The dimensional semispan $\bar{b}/2$ divided by itself becomes the nondimensional semispan $y_t = 1.0$.

The method of calculation is, of course, applicable to other than variable-sweep wing planforms. For instance, fixed straight-tapered sweptback wings can be represented by specifying a pivot axis which coincides with the wing leading-edge apex. Fixed wings with

discontinuous leading-edge sweep can be represented by specifying a pivot axis which coincides with the wing leading-edge sweep discontinuity. In the latter case, $\bar{c}_r'$ may not be known and can be determined by the following relation:

$$\bar{c}_r' = \frac{\cos \Lambda_2}{\cos \Lambda_2'} \bar{c}_r + \left(1 - \frac{\cos \Lambda_2}{\cos \Lambda_2'}\right) \bar{x}_p - \left(k_2' - k_2 \frac{\cos \Lambda_2}{\cos \Lambda_2'}\right) \bar{y}_p \tag{12}$$

The wing geometry relations presented in this section are sufficient for a complete description of a variable-sweep wing as required for a calculation of the camber.

Field-Point Locations

In specifying field-point locations, it is convenient to use streamwise coordinates which are measured from the leading edge of the local chord and are expressed in fractions of that chord

$$\frac{\Delta x_0}{c} = \frac{x_0 - x_{le}}{c} \tag{13}$$

Here x_{le} is the streamwise location of the leading edge of the local chord, measured from the wing leading-edge apex. For variable-sweep wings of the type described in the preceding sections, the field-point coordinates may be calculated with the aid of equation (13) as follows:

For $0 < y_0 \leqq y_k$ and $\sigma' \leqq \sigma \leqq \frac{\pi}{2}$,

$$c = c_r + \left(k_2 - k_1'\right) y_0$$

$$x_0 = \left(\frac{\Delta x_0}{c}\right)\left[c_r + \left(k_2 - k_1'\right) y_0\right] + k_1' y_0$$

For $y_k < y_0 \leqq y_t - c_t \cos \sigma$ and $\sigma' \leqq \sigma \leqq \frac{\pi}{2}$,

$$c = c_r - x_a + \left(k_2 - k_1\right) y_0$$

$$x_0 = \left(\frac{\Delta x_0}{c}\right)\left[c_r - x_a + \left(k_2 - k_1\right) y_0\right] + x_a + k_1 y_0$$

For $y_t - c_t \cos \sigma < y_0 \leqq y_t$ and $\sigma' \leqq \sigma \leqq \frac{\pi}{2}$,

$$c = x_b - x_a + \left(k_3 - k_1\right) y_0$$

$$x_0 = \left(\frac{\Delta x_0}{c}\right)\left[x_b - x_a + \left(k_3 - k_1\right) y_0\right] + x_a + k_1 y_0$$

The foregoing relations are not necessary for a satisfactory specification of field points. Any suitable method of specification may, of course, be used. One other method which was found useful was to specify field-point-coordinate locations on the wing in the fully sweptback position (with the leading edge straight). At the forward sweep positions, the field points were considered to have moved with the wing. A description of some camber results obtained in this way is presented in a subsequent section.

Calculation of Mean Line Camber Ordinates

In addition to the field-point coordinates (x_0,y_0) and the kink coordinates (x_k,y_k), the following quantities are used in the calculation:

$$y_1 = \frac{x_0}{k_1'} \qquad (0 \leqq x_0 \leqq x_k)$$

$$y_1 = \frac{x_0 - x_a}{k_1} \qquad (x_k \leqq x_0 \leqq x_a + k_1 y_t)$$

$$y_2 = \frac{x_0 - c_r}{k_2} \qquad (c_r \leqq x_0)$$

$$y_3 = \frac{x_0 - x_b}{k_3} \qquad \left(x_a + k_1 y_t < x_0 \quad \text{and} \quad \sigma < \frac{\pi}{2}\right)$$

From these values of y, the values of θ are obtained from equation (3), in general, as

$$\theta = \cos^{-1}(-y)$$

so that, for example, $\theta_0 = \cos^{-1}(-y_0)$ and $\theta_k = \cos^{-1}(-y_k)$, etc.

By rewriting equation (7) with the use of equations like equation (B5) for C_n and substituting the summation equations (C1) to (C4), the expression for the mean line camber ordinate becomes

$$z_0 = \frac{1}{\pi \sin \theta_0} \sum_m A_m \sum_s L_{m,s} \tag{14}$$

The summation on m is made over all values of m for which the A_m coefficients are known. The $L_{m,s}$ functions are as follows:

$$L_{m,1} = k_2^2\left[E_m(\theta_2) - E_m\left(\frac{\pi}{2}\right)\right] - k_1^2\left[E_m(\theta_1) - E_m\left(\frac{\pi}{2}\right)\right]$$

$$+ \frac{1}{4}\left(k_2^2\cos^2\theta_2 - k_1^2\cos^2\theta_1\right)D_m(\pi) - \left(k_2^2\cos\theta_2 - k_1^2\cos\theta_1\right)D_m\left(\frac{\pi}{2}\right) \qquad (15)$$

$$L_{m,2} = \frac{1}{4}\left[x_0 - \left(x_a + k_1 y_t\right)\right]^2 D_m(\pi) + k_1\left[x_0 - \left(x_a + k_1 y_t\right)\right]\left[\frac{1}{2}D_m(\pi) - D_m\left(\frac{\pi}{2}\right)\right] \qquad (16)$$

$$L_{m,3} = -k_2^2 E_m(\theta_3) + k_1^2 E_m\left(\frac{\pi}{2}\right) - \left(k_1^2 - k_2^2\right)E_m(\pi)$$

$$- \frac{1}{4}\left(k_1^2 - k_2^2\sin^2\theta_3\right)D_m(\pi) - \left[k_1^2 - k_2^2(1 + \cos\theta_3)\right]D_m\left(\frac{\pi}{2}\right) \qquad (17)$$

$$L_{m,4} = \left(k_1' - k_1\right)\left(x_0 - x_k\right)\left[D_m\left(\theta_k\right) - D_m\left(\frac{\pi}{2}\right) + \frac{1}{2}\left(\cos\theta_k\right)D_m(\pi)\right]$$

$$- \left(k_1'^2 - k_1^2\right)\left[E_m\left(\theta_k\right) - E_m\left(\frac{\pi}{2}\right) + \frac{1}{4}\left(\cos^2\theta_k\right)D_m(\pi) - \left(\cos\theta_k\right)D_m\left(\frac{\pi}{2}\right)\right] \qquad (18)$$

$$L_{m,5} = k_2^2\left[E_m\left(\theta_2\right) - E_m\left(\frac{\pi}{2}\right)\right] - \left(k_2^2\cos\theta_2\right)\left[D_m\left(\frac{\pi}{2}\right) - \frac{1}{4}\left(\cos\theta_2\right)D_m(\pi)\right] \qquad (19)$$

The particular $L_{m,s}$ functions to be used and the values of θ to be inserted in these functions are specified for the various ranges of the field-point locations.

(1) For field points forward of the wing leading-edge kink and the trailing-edge root $\left(0 < x_0 \leqq x_k \leqq c_r \quad \text{or} \quad 0 < x_0 \leqq c_r \leqq x_k\right)$:

$$\sum_s L_{m,s} = L_{m,1}$$

with

$$\theta_1 = \cos^{-1}\left(-\frac{x_0}{k_1'}\right)$$

$$\theta_2 = \frac{\pi}{2}$$

where k_1' is used in $L_{m,1}$ in place of k_1.

(2) For field points forward of the wing leading-edge kink but behind the wing trailing-edge root $\left(c_r < x_0 \leqq x_k\right)$:

$$\sum_s L_{m,s} = L_{m,1}$$

with

$$\theta_1 = \cos^{-1}\left(-\frac{x_0}{k_1'}\right)$$

$$\theta_2 = \cos^{-1}\frac{c_r - x_0}{k_2}$$

and again k_1' is used in $L_{m,1}$ in place of k_1.

(3) For field points behind the wing leading-edge kink but forward of the trailing-edge root and of the outboard leading-edge tip $\left(x_k < x_0 \leqq c_r \leqq x_a + k_1 y_t \text{ or } x_k < x_0 \leqq x_a + k_1 y_t \leqq c_r\right)$:

$$\sum_s L_{m,s} = L_{m,1} + L_{m,4}$$

with

$$\theta_1 = \cos^{-1} \frac{x_a - x_0}{k_1}$$

$$\theta_2 = \frac{\pi}{2}$$

$$\theta_k = \cos^{-1}(-y_k)$$

(4) For field points behind the wing trailing-edge root and of the wing leading-edge kink but forward of the wing leading-edge tip $\left(x_k \leqq c_r < x_0 \leqq x_a + k_1 y_t \text{ or } c_r \leqq x_k < x_0 \leqq x_a + k_1 y_t\right)$

$$\sum_s L_{m,s} = L_{m,1} + L_{m,4}$$

with

$$\theta_1 = \cos^{-1} \frac{x_a - x_0}{k_1}$$

$$\theta_2 = \cos^{-1} \frac{c_r - x_0}{k_2}$$

$$\theta_k = \cos^{-1}(-y_k)$$

(5) For field points behind the wing leading-edge tip and the trailing-edge root, with $\left(\sigma = \frac{\pi}{2}\right)$ streamwise wing tips $\left(c_r \leqq x_a + k_1 y_t < x_0 \leqq c_r + k_2 y_t \text{ or } x_a + k_1 y_t \leqq c_r < x_0 \leqq c_r + k_2 y_t\right)$:

$$\sum_s L_{m,s} = L_{m,1} + L_{m,2} + L_{m,4}$$

with

$$\theta_1 = \pi$$

$$\theta_2 = \cos^{-1} \frac{c_r - x_0}{k_2}$$

$$\theta_k = \cos^{-1}(-y_k)$$

(6) Same as (5) except $\left(\sigma' \leqq \sigma < \frac{\pi}{2}\right)$ wing tips not streamwise $\left(c_r \leqq x_a + k_1 y_t < x_0 \leqq \frac{x_b - c_r}{k_2 - k_3}\right.$ or $\left. x_a + k_1 y_t \leqq c_r < x_0 \leqq \frac{x_b - c_r}{k_2 - k_3}\right)$:

$$\sum_s L_{m,s} = L_{m,2} + L_{m,3} + L_{m,4} + L_{m,5}$$

with

$$\theta_2 = \cos^{-1} \frac{c_r - x_0}{k_2}$$

$$\theta_3 = \cos^{-1} \frac{x_b - x_0}{k_3}$$

$$\theta_k = \cos^{-1}(-y_k)$$

The camber equations given in this section complete the presentation of the method of calculating camber for variable-sweep wings using the sonic slender wing theory. The wing geometry has been specified, field-point locations have been determined, and the camber relations for various regions of the wing have been stated. The way in which the method can be applied to wings of simpler planform has also been indicated. The next section will present camber results which have been obtained for some specific planforms.

Calculated Camber Results

Camber ordinates have been calculated for the variable-sweep planform shown in figures 3 and 4. At the design sweep angle of 75° 58', the leading edge is straight and the wing has an aspect ratio of 1.64. At the most forward sweep of 15° 58', the wing tips are streamwise. Camber results for these two wing sweeps and for a third intermediate sweep angle of 45° 58' are presented in figure 5.

The wing loading imposed for all sweep positions was elliptical spanwise except in the vicinity of the wing tips which were intentionally unloaded. Consequently, the ordinates presented for each wing-sweep position represent the camber required to achieve nearly elliptical span load distribution at that wing sweep. As explained in a preceding section, the variable-sweep wing planform has been idealized in the region of the pivot by extending the inboard and outboard leading edges to a common intersection at the kink point and by extending a straight trailing edge into the center line for all wing-sweep positions.

The camber ordinates are calculated with respect to an orthogonal Cartesian coordinate system with its origin at the leading-edge root of the fixed inboard part of the wing. These ordinates are therefore absolute in that no shear or dihedral variation has been applied to them. The field points (points at which the camber has been calculated) were

located along constant x lines for the wing in the fully swept (75° 58') position. For the other two sweep positions, the field points were maintained in the same relative positions with respect to the local planform geometry so that those points which were located on the outer wing panel moved with the panel as the sweep was varied. (See fig. 4). The camber ordinates in figure 5 have been plotted as a function of the original field-point positions on the variable-sweep wing in the fully swept position. By this method the calculated camber lines for the wing can be traced through the various sweep positions. Of course, only a deformable wing could satisfy the conflicting camber requirements for the various sweep positions. However, by a suitable choice of pivot axis orientation and initial wing shear or dihedral variation in the fully swept design condition, the conflicts may be minimized and a satisfactory compromise may be possible. This aspect of the problem has not been treated herein. For comparison purposes, supersonic (M = 3) camber lines are also shown in figure 5 for the 75° 58' sweep angle. The supersonic camber was calculated by using references 7 to 9.

Mean line camber ordinates were also calculated for a conventional sweptback wing with straight taper and streamwise tips. The wing had an aspect ratio of 8, a taper ratio of 0.3, and a quarter-chord-line sweepback angle of 40°. As mentioned previously, wings of this type can be represented in the equations of the preceding sections by specifying a pivot axis which coincides with the wing leading-edge apex. Camber ordinates are shown in figure 6 for spanwise locations at 0.1, 0.3, 0.5, and 0.8 of the semispan and are compared with ordinates (presented in ref. 10) which were calculated by a different method. In figure 6, the camber ordinates have been adjusted to give a zero camber ordinate along the leading edge. The wing section of the model of reference 10 was formed by distributing standard symmetrical airfoil thickness profiles (NACA 65A-series sections) from reference 11 about the calculated mean line camber ordinates.

A limited appraisal of the value of slender wing theory for design purposes may be obtained from the aerodynamic data of reference 10. The data indicate that some modifications to the basic wing design were necessary to improve aerodynamic performance in the high subsonic speed range. The primary modification was an extension of the inboard leading edge. This extension increased the sweep angle and reduced the thickness ratio and leading-edge camber in that region. The local supersonic flow on the inboard portion of the wing was relieved and the formation of strong shocks which were encountered in that region was delayed by the modification. Further modifications to wings of this type were reported in reference 12 and confirmed the results shown in reference 10.

The wing planform of reference 12 resembled the planform of variable-sweep wings in an intermediate-sweep position, but it was a fixed-geometry wing configuration. As previously mentioned, wings of this type can be represented in the equations of the

preceding section by specifying that the pivot axis coincides with the wing leading-edge kink position and by employing equation (12) to relate $\bar{c}_r'$ to $\bar{c}_r$.

The slender wing (linear) theory for Mach 1 is not considered to be adequate for the calculation of the actual detailed shape of the airfoil section camber for supercritical wings designed for near-sonic speeds. These wings tend to be heavily loaded and have a large region of supercritical flow. Consequently a more elaborate nonlinear transonic analysis in which a separation of camber and thickness effects is not possible or a trial-and-error experimental development is considered to be necessary. Despite this limitation, an application of the linear theory for the prediction of wing twist distribution for wings of this type has been examined.

The results of a twist calculation for a supercritical wing planform designed for near-sonic speeds is presented in figure 7 where the twist angle ϵ was calculated from

$$\tan \epsilon = \left(\frac{z_0}{c}\right)_{le} - \left(\frac{z_0}{c}\right)_{te}$$

The experimental data shown in this figure are based on unpublished results obtained at the NASA Langley Research Center by Charles D. Harris, Charles H. Fox, Jr., Robert T. Taylor, Dennis W. Bartlett, and Richard J. Re. An elliptical spanwise load distribution was assumed for the calculation and was approximately the same as the measured spanwise load distribution. The experimental twist distribution was obtained from structural wing twist data and was corrected for aeroelastic effects. An adjustment for wing incidence and the effect of angle of attack was also made.

A comparison of the twist distribution predicted by the linear theory with that obtained experimentally shows that the linear theory predicts the general magnitude and trend of the spanwise variation of the twist angle. However, for a unit lift coefficient ($C_L = 1.0$), the experimentally determined twist distribution exceeds the calculated results by about 2° to 4° (excluding the immediate region of the kink). An experimentally determined adjustment of the wing incidence angle may therefore be necessary in applying the theory. It should be noted that the experimental results include the effect of a fuselage extending approximately over the inboard 10 percent of the wing; however, fuselage effects were not included in the linear theory prediction.

CONCLUDING REMARKS

A calculation procedure based on slender wing theory at Mach 1 has been derived for the determination of the mean line camber ordinates for polygonal planform wings with lateral symmetry. A uniform chordwise load and a continuous but otherwise arbitrary

spanwise load distribution was assumed. The range of applicability of the results is generally restricted to low lift coefficients and high subsonic speeds for slender wings for which the slenderness parameter βA is small.

Although the slender wing theory for Mach 1 is considered to be inadequate for the calculation of the detailed shape of airfoil section camber for supercritical wings designed for near-sonic speeds, a comparison with experimental results shows that it predicts the general magnitude and trend of the spanwise variation of the twist angle. An experimentally determined adjustment of the wing incidence angle may, however, be necessary in applying the slender wing theory to supercritical wings.

Langley Research Center,
National Aeronautics and Space Administration,
Hampton, Va., June 28, 1971.

APPENDIX A

EVALUATION OF THE B_n FOURIER COEFFICIENTS

The B_n Fourier coefficients for a wing of arbitrary planform with a spanwise load distribution which is everywhere continuous are given by

$$B_n = \frac{2}{\pi}\int_0^{\pi} P^* \sin n\theta \, d\theta \tag{A1}$$

where P^* has been assumed to be an odd function of θ. If the wing has lateral symmetry, that is, symmetry about the x,z plane at $y = 0$, then only odd harmonics will occur in the B_n coefficients. Consequently, equation (A1) may be changed to an integral over the right half of the wing

$$B_n = \frac{4}{\pi}\int_{\pi/2}^{\pi} P^* \sin n\theta \, d\theta \tag{A2}$$

For this case P^* is not only an odd function of θ but is also symmetrical about $\theta = \frac{\pi}{2}$. The further restriction of uniform chordwise load distribution is now introduced so that

$$\Delta C_p = c_l$$

Consequently, equation (2) may be rewritten as

$$P^* = \int_{x_A}^{x_B} c_l \, dx = \left(x_B - x_A\right)c_l \tag{A3}$$

The spanwise distribution of c_l may be expressed in the trigonometric series of equation (11)

$$c_l = \sum_m A_m \sin m\theta \tag{A4}$$

The series for c_l can be a finite trigonometric series or it can be a Fourier series. In the latter case, generally just the first few terms are needed for c_l distributions which are smooth. The use of equation (A4) in equation (A3) yields

$$P^* = \left(x_B - x_A\right)\sum_m A_m \sin m\theta \tag{A5}$$

Equation (A2) for the B_n Fourier coefficients then becomes

$$B_n = \frac{4}{\pi}\int_{\pi/2}^{\pi}(x_B - x_A)\sum_m A_m \sin m\theta \sin n\theta \, d\theta \tag{A6}$$

By interchanging the order of integration and summation, equation (A6) may be rewritten as

$$B_n = \frac{4}{\pi}\sum_m A_m \int_{\pi/2}^{\pi}(x_B - x_A)\sin m\theta \sin n\theta \, d\theta \tag{A7}$$

The type of polygonal wing planform initially to be considered is shown in figure 2. It is a tapered sweptback wing with straight leading and trailing edges and with streamwise tips. In this case the geometric variables for complete planform definition may be expressed in three parameters: aspect ratio A, taper ratio λ, and sweep angle Λ. An extension to more general planform shapes such as those encountered on a variable-sweep wing is given in the main text.

For illustrative purposes, a field point will be considered where a Mach line through the field point intercepts both the leading and trailing edges. In this case, the field point is behind the trailing-edge root $(x = c_r)$ but forward of the leading-edge tip $(x = k_1 y_t)$ where $c_r \leqq x_0 \leqq k_1$, as shown in figure 2. The lower limit x_A in equation (A3) is given by the wing leading edge as $k_1 y$ or $-k_1 \cos\theta$. The points where the Mach line $x = x_0$ through the field point intercepts the wing edges are designated as $y_1 = -\cos\theta_1$ for the leading edge and $y_2 = -\cos\theta_2$ for the trailing edge. Consequently, for span stations inboard of θ_2, the upper limit x_B is $c_r - k_2 \cos\theta$, and for span stations between θ_1 and θ_2 the upper limit is x_0. After substitution of the appropriate limits, equation (A7) for the Fourier coefficients becomes

$$B_n = \frac{4}{\pi}\sum_m A_m \left\{\int_{\pi/2}^{\theta_2}\left[(k_1 - k_2)\cos\theta \sin m\theta \sin n\theta + c_r \sin m\theta \sin n\theta\right]d\theta \right.$$

$$\left. + \int_{\theta_2}^{\theta_1}(k_1 \cos\theta \sin m\theta \sin n\theta + x_0 \sin m\theta \sin n\theta)d\theta\right\} \tag{A8}$$

Upon integration and substitution of the relation

$$x_0 = -k_1 \cos\theta_1 = c_r - k_2 \cos\theta_2 \tag{A9}$$

which is valid in the region $c_r \leqq x_0 \leqq k_1$, equation (A8) becomes

$$B_n = -\frac{4}{\pi}\sum_m A_m\left(k_1\left\{\left[\cos\theta_1 F(\theta_1) - G(\theta_1)\right] - \left[\cos\theta_1 F\left(\frac{\pi}{2}\right) - G\left(\frac{\pi}{2}\right)\right]\right\}\right.$$

$$\left. - k_2\left\{\left[\cos\theta_2 F(\theta_2) - G(\theta_2)\right] - \left[\cos\theta_2 F\left(\frac{\pi}{2}\right) - G\left(\frac{\pi}{2}\right)\right]\right\}\right) \tag{A10}$$

where

$$F(\theta) = \frac{1}{2}\left[\frac{\sin(n-m)\theta}{n-m} - \frac{\sin(n+m)\theta}{n+m}\right] \tag{A11}$$

$$G(\theta) = \frac{1}{4}\left[\frac{\sin(n-m+1)\theta}{n-m+1} + \frac{\sin(n-m-1)\theta}{n-m-1} - \frac{\sin(n+m+1)\theta}{n+m+1} - \frac{\sin(n+m-1)\theta}{n+m-1}\right] \tag{A12}$$

Simple indeterminate forms which are encountered in equations (A11) and (A12) may be evaluated as follows:

$$\lim_{p \to 0} \frac{\sin p\theta}{p} = \theta \tag{A13}$$

It should be restated here that the B_n Fourier coefficients obtained from equation (A10) are limited in application because of the assumptions inherent in the derivation. Equation (A10) is restricted to straight-edged sweptback wings with lateral symmetry and uniform chordwise load and is specifically formulated for field points in the region $c_r \leqq x_0 \leqq k_1$. These limitations are carried over to the evaluation of the C_n coefficients in appendix B.

APPENDIX B

EVALUATION OF THE C_n COEFFICIENTS

The C_n coefficients are evaluated from equation (8) by using equations (A9) and (A10) and therefore are subject to the same restrictions as were the B_n Fourier coefficients evaluated in appendix A. That is, they are for a polygonal planform (straight-edged) wing with lateral symmetry and for a uniform chordwise load. The field point is also located in the region $c_r \leqq x_0 \leqq k_1$. The extension to wings with less restricted planform and field-point location is given in the text.

With the substitution of equation (A10) into equation (8), the expression for the C_n coefficients becomes

$$C_n = -\frac{4}{\pi}\sum_m A_m \left(k_1 \int_0^{x_0} \left\{ \left[\cos\theta_1 \, F(\theta_1) - G(\theta_1) \right] - \left[\cos\theta_1 \, F\left(\frac{\pi}{2}\right) - G\left(\frac{\pi}{2}\right) \right] \right\} dx \right.$$

$$\left. - k_2 \int_0^{x_0} \left\{ \left[\cos\theta_2 \, F(\theta_2) - G(\theta_2) \right] - \left[\cos\theta_2 \, F\left(\frac{\pi}{2}\right) - G\left(\frac{\pi}{2}\right) \right] \right\} dx \right) \tag{B1}$$

From equation (A9) it can be seen that

$$dx_0 = k_1 \sin\theta_1 \, d\theta_1 \qquad \left(\frac{\pi}{2} \leqq \theta \leqq \theta_1 \right) \tag{B2}$$

and

$$dx_0 = k_2 \sin\theta_2 \, d\theta_2 \qquad \left(\frac{\pi}{2} \leqq \theta \leqq \theta_2 \right) \tag{B3}$$

Substituting equations (B2) and (B3) into the first and second integrals, respectively, of equation (B1) gives the expression for C_n

$$C_n = -\frac{4}{\pi}\sum_m A_m \left(k_1^2 \int_{\pi/2}^{\theta_1} \left\{ \left[\cos\theta_1 \, F(\theta_1) - G(\theta_1) \right] - \left[\cos\theta_1 \, F\left(\frac{\pi}{2}\right) - G\left(\frac{\pi}{2}\right) \right] \right\} \sin\theta_1 \, d\theta_1 \right.$$

$$\left. - k_2^2 \int_{\pi/2}^{\theta_2} \left\{ \left[\cos\theta_2 \, F(\theta_2) - G(\theta_2) \right] - \left[\cos\theta_2 \, F\left(\frac{\pi}{2}\right) - G\left(\frac{\pi}{2}\right) \right] \right\} \sin\theta_2 \, d\theta_2 \right) \tag{B4}$$

Integration of equation (B4) yields

$$C_n = \frac{4}{\pi} \sum_m A_m \left(k_1^2 \left\{ \frac{1}{8} \left[H(\theta_1) - H\left(\frac{\pi}{2}\right) \right] - \left[I(\theta_1) - I\left(\frac{\pi}{2}\right) \right] \right\} \right.$$

$$\left. - k_2^2 \left\{ \frac{1}{8} \left[H(\theta_2) - H\left(\frac{\pi}{2}\right) \right] - \left[I(\theta_2) - I\left(\frac{\pi}{2}\right) \right] \right\} \right) \tag{B5}$$

where

$$H(\theta) = - \frac{\sin(n + m + 2)\theta}{(n + m)(n + m + 1)(n + m + 2)} + \frac{2 \sin(n + m)\theta}{(n + m - 1)(n + m)(n + m + 1)}$$

$$- \frac{\sin(n + m - 2)\theta}{(n + m - 2)(n + m - 1)(n + m)} - \frac{2 \sin(n - m)\theta}{(n - m - 1)(n - m)(n - m + 1)}$$

$$+ \frac{\sin(n - m + 2)\theta}{(n - m)(n - m + 1)(n - m + 2)} + \frac{\sin(n - m - 2)\theta}{(n - m - 2)(n - m - 1)(n - m)} \tag{B6}$$

$$I(\theta) = \cos \theta \left[\frac{1}{2} \cos \theta \, F\left(\frac{\pi}{2}\right) - G\left(\frac{\pi}{2}\right) \right] \tag{B7}$$

The simple indeterminate forms which are encountered in equation (B6) may be evaluated by using the form of equation (A13) as follows:

$$\lim_{(n-m) \to 0} \left[\frac{\sin(n - m)\theta}{(n - m - 1)(n - m)(n - m + 1)} \right] = -\theta$$

$$\lim_{(n+m-2) \to 0} \left[\frac{\sin(n + m - 2)\theta}{(n + m - 2)(n + m - 1)(n + m)} \right] = \frac{\theta}{2}$$

$$\lim_{(n-m+2) \to 0} \left[\frac{\sin(n - m + 2)\theta}{(n - m)(n - m + 1)(n - m + 2)} \right] = \frac{\theta}{2}$$

$$\lim_{(n-m-2) \to 0} \left[\frac{\sin(n - m - 2)\theta}{(n - m - 2)(n - m - 1)(n - m)} \right] = \frac{\theta}{2}$$

$$\lim_{(n-m) \to 0} \left[\frac{\sin(n - m + 2)\theta}{(n - m)(n - m + 1)(n - m + 2)} + \frac{\sin(n - m - 2)\theta}{(n - m - 2)(n - m - 1)(n - m)} \right] = \theta \cos 2\theta - \frac{3}{2} \sin 2\theta$$

Once again it should be stated that the limitations inherent in the B_n Fourier coefficients represented by equation (A10) also apply to the C_n coefficients represented by equation (B5). The derivation of these equations, however, is indicative of the methods used for extension to less restricted planform and field-point locations. The limitation to uniform chordwise load, however, is retained throughout the analysis.

APPENDIX C

ANALYTICAL SUMMATION OF SERIES

The series summations over n of equations (6) and (7) with the use of equations (A10) and (B5), respectively, are not rapidly convergent and generally require a large number of terms to be summed before a satisfactory numerical result is achieved. With equation (B5) for the C_n coefficients substituted into equation (7) and with the order of the summations over n and m interchanged, the summation over n may be obtained independently of the summation over m. An example of the methods used to obtain one of the summation terms is presented in appendix D. Similar methods are applicable to the other summation terms. The results of the summation are summarized as follows:

$$\sum_{n=1}^{\infty} n \sin n\theta_0 \left[\cos\ \theta\ F(\theta) - G(\theta)\right] = D_m(\theta) \tag{C1}$$

$$\sum_{n=1}^{\infty} n \sin n\theta_0\ F\left(\frac{\pi}{2}\right) = -\frac{1}{2} D_m(\pi) \tag{C2}$$

$$\sum_{n=1}^{\infty} n \sin n\theta_0\ G\left(\frac{\pi}{2}\right) = -D_m\left(\frac{\pi}{2}\right) \tag{C3}$$

$$\sum_{n=1}^{\infty} n \sin n\theta_0\ H(\theta) = E_m(\theta) \tag{C4}$$

where

$$D_m(\theta) = \frac{m}{2} \cos\ \theta \left\{ \frac{1}{4} \cos m\theta_0 \log \left[\frac{\sin^2(\theta_0 + \theta)}{\sin^2(\theta_0 - \theta)}\right] + 2 \sum_{r=1}^{\frac{m+1}{2}} \frac{\sin 2r\theta \sin(m - 2r)\theta}{2r} + \frac{2 \sin\ \theta_0 \sin(m + 1)\theta}{m + 1} + \theta \sin m\theta_0 \right\}$$

$$+ \left(m \cos m\theta_0 \cos\ \theta_0 - \sin m\theta_0 \sin\ \theta_0\right) \left\{ \frac{1}{8} \log \left[\frac{\sin(\theta_0 + \theta)}{\sin(\theta_0 - \theta)} \frac{1 - \cos(\theta_0 - \theta)}{1 - \cos(\theta_0 + \theta)}\right]^2 + \sum_{r=1}^{\frac{m+1}{2}} \frac{\sin(2r - 1)\theta_0 \sin(2r - 1)\theta}{2r - 1} \right\}$$

$$- \frac{m - 1}{2m} \sin m\theta \sin\ \theta_0 - \left(m \sin m\theta_0 \cos\ \theta_0 + \cos m\theta_0 \sin\ \theta_0\right) \left[\sum_{r=1}^{\frac{m+1}{2}} \frac{\cos(2r - 1)\theta_0 \sin(2r - 1)\theta}{2r - 1} \right]$$

$$(\theta \neq \theta_0) \tag{C5}$$

$$-\frac{1}{2}D_m(\pi) = \frac{m\pi}{4}\sin m\theta \tag{C6}$$

$$E_m(\theta) = \frac{1}{8}\left[m\left(\cos^2\theta + \cos^2\theta_0\right)\cos m\theta_0 - 2\cos\theta_0 \sin\theta_0 \sin m\theta_0\right]\left\{\frac{1}{2}\log\left[\frac{\sin^2(\theta_0 + \theta)}{\sin^2(\theta_0 - \theta)}\right]\right.$$

$$\left. - 4\sum_{r=1}^{\frac{m+1}{2}} \frac{\sin 2r\theta_0 \sin 2r\theta}{2r}\right\} + \frac{1}{4}\cos\theta\left(m\cos m\theta_0 \cos\theta_0 - \sin m\theta_0 \sin\theta_0\right)$$

$$\times\left\{\frac{1}{2}\log\left[\frac{\sin^2(\theta_0 + \theta)}{\sin^2(\theta_0 - \theta)}\right] + \log\left[\frac{1 - \cos(\theta_0 - \theta)}{1 - \cos(\theta_0 + \theta)}\right] + 4\sum_{r=1}^{\frac{m+1}{2}} \frac{\sin(2r-1)\theta_0 \sin(2r-1)\theta}{2r-1}\right\}$$

$$+ \frac{1}{8}\left[m\sin m\theta_0\left(\cos^2\theta + \cos^2\theta_0\right) + 2\sin\theta_0\cos\theta_0\cos m\theta_0\right]$$

$$\times\left[2\theta + 4\sum_{r=1}^{\frac{m+1}{2}} \frac{\cos 2r\theta_0 \sin 2r\theta}{2r}\right] - \frac{1}{4}\cos\theta\left(m\sin m\theta_0\cos\theta_0 + \cos m\theta_0\sin\theta_0\right)$$

$$\times\left[4\sum_{r=1}^{\frac{m+1}{2}} \frac{\cos(2r-1)\theta_0 \sin(2r-1)\theta}{2r-1}\right]$$

$$+ \frac{1}{8}(m-2)\left[\frac{\sin(m-1)\theta\sin\theta_0}{m-1} + \frac{\sin(m+1)\theta\sin 3\theta_0}{m+1}\right] - \frac{1}{2}\frac{(m-1)}{m}\cos\theta\sin m\theta_0\sin\theta_0$$

$$+ \frac{1}{4}\frac{m(2+\cos 2\theta)}{m+1}\sin(m+1)\theta\sin\theta_0 \qquad (\theta \neq \theta_0) \tag{C7}$$

$$E_m(\theta) = \frac{1}{4}\cos\theta_0\left(m\cos\theta_0\cos m\theta_0 - \sin\theta_0\sin m\theta_0\right)\left[\log\left(\cos^2\theta_0\right) - 4\sum_{r=1}^{m+1}\frac{(-1)^r\sin^2 r\theta_0}{r}\right]$$

$$+\frac{1}{4}\cos\theta_0\left(m\cos\theta_0\sin m\theta_0 + \sin\theta_0\cos m\theta_0\right)\left(2\theta_0 + 4\sum_{r=1}^{m+1}\frac{(-1)^r\cos r\theta_0\sin r\theta_0}{r}\right)$$

$$+\frac{1}{8}(m-2)\left[\frac{\sin(m-1)\theta_0\sin\theta_0}{m-1} + \frac{\sin(m+1)\theta_0\sin 3\theta_0}{m+1}\right]$$

$$-\frac{(m-1)}{2m}\cos\theta_0\sin m\theta_0\sin\theta_0 + \frac{m(2+\cos 2\theta_0)}{4(m+1)}\sin(m+1)\theta_0\sin\theta_0$$

$$(\theta = \theta_0) \qquad \text{(C8)}$$

and the indeterminate form in equations (C7) and (C8) may be evaluated as follows:

$$\lim_{m \to 1}\left[\frac{\sin(m-1)\theta_0\sin\theta_0}{m-1}\right] = \theta_0\sin\theta_0$$

To assist in numerical calculations, the functions $\frac{D_m(\theta)}{m\sin m\theta_0}$ and $\frac{E_m(\theta)}{m\sin m\theta_0}$ are presented in graphical form in figures 8 and 9 for odd values of m up to $m = 39$. A curve for m approaching ∞ has been added to show the limit toward which these functions tend as m grows very large. Figures 8 and 9 have been prepared for fixed values of y_0 corresponding to values of θ_0 at 7.5° increments from 90° to 172.5°. The curves at $\theta_0 = 120^\circ$ for the odd values of m which are multiples of 3 have been deleted from figures 8(e) and 9(e). They are presented separately in figure 10 for $D_m(\theta)$ and in figure 11 for $E_m(\theta)$. These extra figures are necessary because $\sin m\theta_0$ equals zero in the denominator of the functions presented in figures 8 and 9 at $\theta_0 = 120^\circ$ for these values of m.

APPENDIX D

DERIVATION OF ANALYTICAL SUMMATION OF SERIES

The derivation of the closed-form result (eq. (C5)) of the summation expressed in equation (C1) is shown in detail. Equation (C1) is rewritten

$$D_m(\theta) = \sum_{n=1}^{\infty} n \sin n\theta_0 \left[\cos\ \theta\ F(\theta) - G(\theta)\right] \tag{D1}$$

The substitution of the expression for $F(\theta)$ from equation (A11) and for $G(\theta)$ from equation (A12) into equation (D1) yields

$$D_m(\theta) = \sum_{n=1}^{\infty} n \sin n\theta_0 \left\{ \frac{1}{2} \cos\ \theta \left[\frac{\sin(n - m)\theta}{n - m} - \frac{\sin(n + m)\theta}{n + m} \right] \right.$$

$$\left. - \frac{1}{4} \left[\frac{\sin(n - m + 1)\theta}{n - m + 1} + \frac{\sin(n - m - 1)\theta}{n - m - 1} - \frac{\sin(n + m + 1)\theta}{n + m + 1} - \frac{\sin(n + m - 1)\theta}{n + m - 1} \right] \right\} \tag{D2}$$

Equation (D2) may be simplified to

$$D_m(\theta) = \sum_{n=1}^{\infty} \sin n\theta_0 \left\{ \frac{m}{2} \cos\ \theta \left[\frac{\sin(n - m)\theta}{n - m} + \frac{\sin(n + m)\theta}{n + m} \right] \right.$$

$$\left. - \frac{m - 1}{4} \left[\frac{\sin(n - m + 1)\theta}{n - m + 1} + \frac{\sin(n + m - 1)\theta}{n + m - 1} \right] - \frac{m + 1}{4} \left[\frac{\sin(n - m - 1)\theta}{n - m - 1} + \frac{\sin(n + m + 1)\theta}{n + m + 1} \right] \right\} \tag{D3}$$

As previously mentioned, if the wing has lateral symmetry, then only odd values of n occur. Consequently, with the substitution of $n = 2r - 1$ where r takes on consecutive integer values, equation (D3) may be rewritten as

$$D_m(\theta) = \sum_{r=1}^{\infty} \sin(2r - 1)\theta_0 \left\{ \frac{m}{2} \cos\ \theta \left[\frac{\sin(2r - m - 1)\theta}{2r - m - 1} + \frac{\sin(2r + m - 1)\theta}{2r + m - 1} \right] \right.$$

$$\left. - \frac{m - 1}{4} \left[\frac{\sin(2r - m)\theta}{2r - m} + \frac{\sin(2r + m - 2)\theta}{2r + m - 2} \right] - \frac{m + 1}{4} \left[\frac{\sin(2r - m - 2)\theta}{2r - m - 2} + \frac{\sin(2r + m)\theta}{2r + m} \right] \right\} \tag{D4}$$

After rearranging and combining terms, equation (D4) becomes

$$D_m(\theta) = \frac{m}{2}\cos\theta\left\{\cos m\theta_0\left[\sum_{r=1}^{\infty}\frac{\cos 2r(\theta_0 - \theta)}{2r} - \sum_{r=1}^{\infty}\frac{\cos 2r(\theta_0 + \theta)}{2r} - \sum_{r=1}^{\frac{m+1}{2}}\frac{\cos 2r(\theta_0 - \theta)}{2r}\right.\right.$$

$$\left. + \sum_{r=1}^{\frac{m+1}{2}}\frac{\cos 2r(\theta_0 + \theta)}{2r} + \frac{\cos(m+1)(\theta_0 - \theta)}{m+1} - \frac{\cos(m+1)(\theta_0 + \theta)}{m+1}\right]$$

$$+ \sin m\theta_0\left[\sum_{r=1}^{\frac{m+1}{2}}\frac{\sin 2r(\theta_0 + \theta)}{2r} - \sum_{r=1}^{\frac{m+1}{2}}\frac{\sin 2r(\theta_0 - \theta)}{2r}\right.$$

$$\left.\left. - \frac{\sin(m+1)(\theta_0 + \theta)}{m+1} + \frac{\sin(m+1)(\theta_0 - \theta)}{m+1} + \theta\right]\right\}$$

$$- \left(m\cos m\theta_0\cos\theta_0 - \sin m\theta_0\sin\theta_0\right)\left[\frac{1}{2}\sum_{r=1}^{\infty}\frac{\cos(2r-1)(\theta_0 - \theta)}{2r-1}\right.$$

$$\left. - \frac{1}{2}\sum_{r=1}^{\infty}\frac{\cos(2r-1)(\theta_0 + \theta)}{2r-1} - \sum_{r=1}^{\frac{m+1}{2}}\frac{\sin(2r-1)\theta_0\sin(2r-1)\theta}{2r-1}\right] - \frac{m-1}{2m}\sin m\theta\sin\theta_0$$

$$- \left(m\sin m\theta_0\cos\theta_0 + \cos m\theta_0\sin\theta_0\right)\left[\sum_{r=1}^{\frac{m+1}{2}}\frac{\cos(2r-1)\theta_0\sin(2r-1)\theta}{2r-1}\right] \qquad \text{(D5)}$$

The following summation is presented in reference 13:

$$\sum_{r=1}^{\infty}\frac{\cos r\theta}{r} = \frac{1}{2}\log\left[\frac{1}{2(1-\cos\theta)}\right] \qquad (0 < \theta < 2\pi) \qquad \text{(D6)}$$

From equation (D6), the following summation may be obtained:

$$\sum_{r=1}^{\infty}\frac{\cos 2r\theta}{2r} = \frac{1}{4}\log\left[\frac{1}{2(1-\cos 2\theta)}\right] \qquad (0 < \theta < \pi) \qquad \text{(D7)}$$

Equation (D7) may be rewritten as

$$\sum_{r=1}^{\infty} \frac{\cos 2r\theta}{2r} = -\frac{1}{4}\log(4 \sin^2\theta) \qquad (0 < \theta < \pi) \qquad \text{(D8)}$$

The series of equation (D6) may be written as the sum of two series

$$\sum_{r=1}^{\infty} \frac{\cos r\theta}{r} = \sum_{r=1}^{\infty} \frac{\cos(2r-1)\theta}{2r-1} + \sum_{r=1}^{\infty} \frac{\cos 2r\theta}{2r} \qquad \text{(D9)}$$

The substitution of equations (D6) and (D8) into equation (D9) yields

$$\sum_{r=1}^{\infty} \frac{\cos(2r-1)\theta}{2r-1} = \frac{1}{4}\log\left(\frac{\sin\theta}{1-\cos\theta}\right)^2 \qquad (0 < \theta < \pi) \qquad \text{(D10)}$$

The cosine series of equations (D8) and (D10) and the functions they represent are even functions of θ and are periodic in intervals of 2π. Consequently, the intervals of convergence of equations (D8) and (D10) may be written

$$-\pi < \theta < 0, \quad 0 < \theta < \pi, \quad \pi < \theta < 2\pi$$

It is therefore seen that, in these two equations, the series converges to the function everywhere except at $\theta = 0$ and at $\theta = \pm p\pi$ where p is any integer.

With the use of equations (D8) and (D10), the infinite series in equation (D5) may be written as

$$\sum_{r=1}^{\infty} \frac{\cos 2r(\theta_0 - \theta)}{2r} - \sum_{r=1}^{\infty} \frac{\cos 2r(\theta_0 + \theta)}{2r} = \frac{1}{4}\log\left[\frac{\sin^2(\theta_0 + \theta)}{\sin^2(\theta_0 - \theta)}\right] \qquad \text{(D11)}$$

and

$$\sum_{r=1}^{\infty} \frac{\cos(2r-1)(\theta_0 - \theta)}{2r-1} - \sum_{r=1}^{\infty} \frac{\cos(2r-1)(\theta_0 + \theta)}{2r-1} = \frac{1}{4}\log\left[\frac{\sin(\theta_0 - \theta)}{\sin(\theta_0 + \theta)}\,\frac{1-\cos(\theta_0 + \theta)}{1-\cos(\theta_0 - \theta)}\right]^2 \qquad \text{(D12)}$$

In equations (D11) and (D12), the range of the angle arguments are (since, in general, $\frac{\pi}{2} \leqq \theta \leqq \pi$) $-\frac{\pi}{2} \leqq (\theta_0 - \theta) \leqq \frac{\pi}{2}$ and $\pi \leqq (\theta_0 + \theta) \leqq 2\pi$. Therefore, the use of equations (D11) and (D12) in equation (D5) is valid everywhere except at $\theta = \theta_0$.

Substitution of equations (D11) and (D12) into equation (D5) yields, after simplification,

$$D_m(\theta) = \frac{m}{2}\cos\theta\left\{\frac{1}{4}\cos m\theta_0 \log\left[\frac{\sin^2(\theta_0 + \theta)}{\sin^2(\theta_0 - \theta)}\right] + 2\sum_{r=1}^{\frac{m+1}{2}} \frac{\sin 2r\theta \sin(m - 2r)\theta}{2r} + \frac{2\sin\theta_0 \sin(m+1)\theta}{m+1} + \theta \sin m\theta_0\right\}$$

$$+ \left(m\cos m\theta_0 \cos\theta_0 - \sin m\theta_0 \sin\theta_0\right)\left\{\frac{1}{8}\log\left[\frac{\sin(\theta_0 + \theta)}{\sin(\theta_0 - \theta)}\frac{1 - \cos(\theta_0 - \theta)}{1 - \cos(\theta_0 + \theta)}\right]^2\right.$$

$$\left. + \sum_{r=1}^{\frac{m+1}{2}} \frac{\sin(2r-1)\theta_0 \sin(2r-1)\theta}{2r-1}\right\} - \frac{m-1}{2m}\sin m\theta \sin\theta_0$$

$$- \left(m\sin m\theta_0 \cos\theta_0 + \cos m\theta_0 \sin\theta_0\right)\left[\sum_{r=1}^{\frac{m+1}{2}} \frac{\cos(2r-1)\theta_0 \sin(2r-1)\theta}{2r-1}\right] \qquad (\theta \neq \theta_0) \qquad \text{(D13)}$$

Equation (D13) is the same as equation (C5). The other summation expressions which are represented by equations (C7) and (C8) may be obtained in a similar manner.

APPENDIX E

CALCULATION OF THE A_m COEFFICIENTS

The desired wing spanwise load distribution is considered to be known so that, for a given planform, the spanwise distribution of section lift coefficient c_l is also known. If an analytical expression for the c_l distribution is known, then the A_m coefficients of equation (11) can be found by a Fourier expansion. However, if the c_l distribution is known only numerically, then the A_m coefficients may be approximated by simple numerical methods for all but the most irregularly shaped c_l distributions. Two such methods are the 17-point odd harmonic numerical method for the sine terms presented in reference 14, and the method in reference 11.

The A_m coefficients for elliptical spanwise load (cc_l) distribution on straight-tapered wings with streamwise tips may be obtained as follows:

$$A_m = \frac{1}{\pi}\int_{-\pi}^{\pi} c_l \sin m\theta \, d\theta = \frac{4}{\pi}\int_{0}^{\pi/2} c_l \sin m\theta \, d\theta \tag{E1}$$

where, for elliptical spanwise load

$$cc_l = \frac{2}{\pi} c_r(1 + \lambda)C_L \sin \theta \tag{E2}$$

In the range of θ from 0 to $\frac{\pi}{2}$, the chord distribution may be expressed as

$$c = c_r\left[1 - (1 - \lambda)\cos \theta\right] \qquad \left(0 \leqq \theta \leqq \frac{\pi}{2}\right) \tag{E3}$$

Substituting equations (E2) and (E3) into equation (E1) yields

$$A_m = \frac{8}{\pi^2}(1 + \lambda)C_L \int_{0}^{\pi/2} \frac{\sin \theta \sin m\theta}{1 - (1 - \lambda)\cos \theta} \, d\theta \tag{E4}$$

The solution for the integral of equation (E4) can be written in the recursion form

$$\frac{A_m}{C_L} = \frac{4}{\pi}\frac{1 + \lambda}{1 - \lambda}\left(K_{m-1} - K_{m+1}\right) \tag{E5}$$

and the recurring K_m functions are evaluated

$$K_0 = \frac{1 - \lambda}{\pi\sqrt{\lambda(2 - \lambda)}}\left(\frac{\pi}{2} + \sin^{-1}\left|1 - \lambda\right|\right)$$

$$K_1 = \frac{K_0}{1 - \lambda} - \frac{1}{2}$$

$$K_{m-1} + K_{m+1} = -\frac{2}{m\pi}\sin\frac{m\pi}{2} + \frac{2}{1 - \lambda}K_m$$

Table 1 presents values of A_m/C_L for values of λ from 0 to 1.0. The values of A_m/C_L for $\lambda = 0$ are for a wing with pointed tips and do not represent a realistically possible lift coefficient distribution. They are included in the table only to indicate limiting values of A_m/C_L as $\lambda \to 0$. In general, the first few entries in the table (at the lowest values of m) were obtained with the recursion formula of equation (E5). At the higher values of m, the table entries were obtained by numerical methods.

The method of solution for camber presented in this report is not well suited for use where a uniform spanwise section lift coefficient distribution is desired. However, approximate results can be obtained with the A_m/C_L values presented in table 2 which were computed by the method of reference 11. The values of $4/\pi m$ obtained by Fourier expansion for a uniform c_l distribution are included in the table for comparison purposes.

REFERENCES

1. Jones, Robert T.: Properties of Low-Aspect-Ratio Pointed Wings at Speeds Below and Above the Speed of Sound. NACA Rep. 835, 1946. (Supersedes NACA TN 1032.)

2. Heaslet, Max. A.; Lomax, Harvard; and Spreiter, John R.: Linearized Compressible-Flow Theory for Sonic Flight Speeds. NACA Rep. 956, 1950. (Supersedes NACA TN 1824.)

3. Heaslet, Max. A.; and Lomax, Harvard: Supersonic and Transonic Small Perturbation Theory. Vol. VI of High Speed Aerodynamics and Jet Propulsion, W. R. Sears, ed., Princeton Univ. Press, 1954, pp. 122-344.

4. Jones, Robert T.; and Cohen, Doris: Aerodynamics of Wings at High Speeds. Vol. VII of High Speed Aerodynamics and Jet Propulsion, A. F. Donovan and H. R. Lawrence, eds., Princeton Univ. Press, 1957, pp. 3-243.

5. Glauert, H.: The Elements of Aerofoil and Airscrew Theory. Cambridge Univ. Press, 1937.

6. Churchill, Ruel V.: Fourier Series and Boundary Value Problems. Second ed., McGraw-Hill Book Co., Inc., c.1963.

7. Tucker, Warren A.: A Method for the Design of Sweptback Wings Warped To Produce Specified Flight Characteristics at Supersonic Speeds. NACA Rep. 1226, 1955. (Supersedes NACA RM L51F08.)

8. Grant, Frederick C.: The Proper Combination of Lift Loadings for Least Drag on a Supersonic Wing. NACA Rep. 1275, 1956. (Supersedes NACA TN 3533.)

9. Brown, Clinton E.; and McLean, Francis E.: The Problem of Obtaining High Lift-Drag Ratios at Supersonic Speeds. J. Aero/Space Sci., vol. 26, no. 5, May 1959, pp. 298-302.

10. Heath, Atwood R., Jr.: Longitudinal Aerodynamic Characteristics of a High-Subsonic-Speed Transport Airplane Model With a Cambered 40° Sweptback Wing of Aspect Ratio 8 at Mach Numbers to 0.96. NASA TN D-218, 1960.

11. Abbott, Ira H.; and Von Doenhoff, Albert E.: Theory of Wing Sections. Dover Publ., Inc., 1959.

12. Re, Richard J.; and Stumbris, Gunars: An Investigation at Mach Numbers From 0.40 to 1.00 of a Model With a Wing Having Inboard Sections Cambered for Mach 1.2. NASA TN D-3419, 1966.

13. Adams, Edwin P.; and Hippisley, R. L.: Smithsonian Mathematical Formulae and Tables of Elliptic Functions. First reprint, Smithsonian Misc. Collect., vol. 74, no. 1, 1939.

14. Lipka, Joseph: Graphical and Mechanical Computation. John Wiley & Sons, Inc., 1918.

TABLE 1.- A_m/C_L FOR ELLIPTICAL SPANWISE LOAD DISTRIBUTION ON STRAIGHT-TAPERED WINGS

m	Values of A_m/C_L for λ of –											
	0	0.05	0.10	0.20	0.30	0.40	0.50	0.60	0.70	0.80	0.90	1.0
1	2.08381	1.54564	1.42881	1.32519	1.28014	1.25886	1.24988	1.24808	1.25080	1.25647	1.26416	$4/\pi$
3	2.62419	1.14767	.84793	.56147	.40690	.30376	.22710	.16621	.11563	.07224	.03411	0
5	2.51611	.52892	.27009	.08838	.02343	-.00433	-.01588	-.01913	-.01768	-.01338	-.00728	0
7	2.56243	.30939	.13437	.04572	.02426	.01707	.01376	.01141	.00908	.00644	.00342	0
9	2.53669	.14392	.03667	-.00215	-.00771	-.00828	-.00767	-.00664	-.00532	-.00378	-.00200	0
11	2.55307	.08718	.02484	.00830	.00639	.00574	.00513	.00440	.00352	.00249	.00132	0
13	2.54174	.03748	.00245	-.00414	-.00435	-.00407	-.00365	-.00312	-.00250	-.00177	-.00093	0
15	2.55005	.02570	.00637	.00358	.00330	.00305	.00273	.00234	.00187	.00132	.00070	0
17	2.54369	.00882	-.00166	-.00266	-.00256	-.00237	-.00212	-.00181	-.00145	-.00102	-.00054	0
19	2.54871	.00831	.00265	.00216	.00205	.00190	.00170	.00145	.00116	.00082	.00043	0
21	2.54465	.00136	-.00164	-.00176	-.00168	-.00155	-.00139	-.00118	-.00094	-.00067	-.00035	0
23	2.54800	.00319	.00158	.00147	.00140	.00129	.00116	.00099	.00079	.00056	.00029	0
25	2.54518	-.00042	-.00126	-.00124	-.00118	-.00109	-.00098	-.00083	-.00066	-.00047	-.00025	0
27	2.54758	.00157	.00111	.00107	.00101	.00094	.00084	.00072	.00057	.00040	.00021	0
29	2.54551	-.00072	-.00095	-.00092	-.00088	-.00081	-.00072	-.00062	-.00049	-.00035	-.00018	0
31	2.54731	.00097	.00084	.00081	.00077	.00071	.00063	.00054	.00043	.00030	.00016	0
33	2.54573	-.00068	-.00074	-.00072	-.00068	-.00063	-.00056	-.00048	-.00038	-.00027	-.00014	0
35	2.54713	.00069	.00066	.00064	.00060	.00056	.00050	.00042	.00034	.00024	.00013	0
37	2.54588	-.00057	-.00059	-.00057	-.00054	-.00050	-.00044	-.00038	-.00030	-.00021	-.00011	0
39	2.54700	.00054	.00053	.00051	.00048	.00045	.00040	.00034	.00027	.00019	.00010	0
.	.	.	.	.	.	.	.	.	.	.	.	.
.	.	.	.	.	.	.	.	.	.	.	.	.
.	.	.	.	.	.	.	.	.	.	.	.	.
∞	$8/\pi$	0	0	0	0	0	0	0	0	0	0	0

TABLE 2.- A_m/C_L FOR UNIFORM c_l DISTRIBUTION

m	A_m/C_L	$4/\pi m$
1	1.27062	1.27324
3	.41652	.42441
5	.24142	.25465
7	.16318	.18189
9	.11708	.14147
11	.08542	.11575
13	.06128	.09794
15	.04142	.08488
17	.02402	.07490
19	.00788	.06701

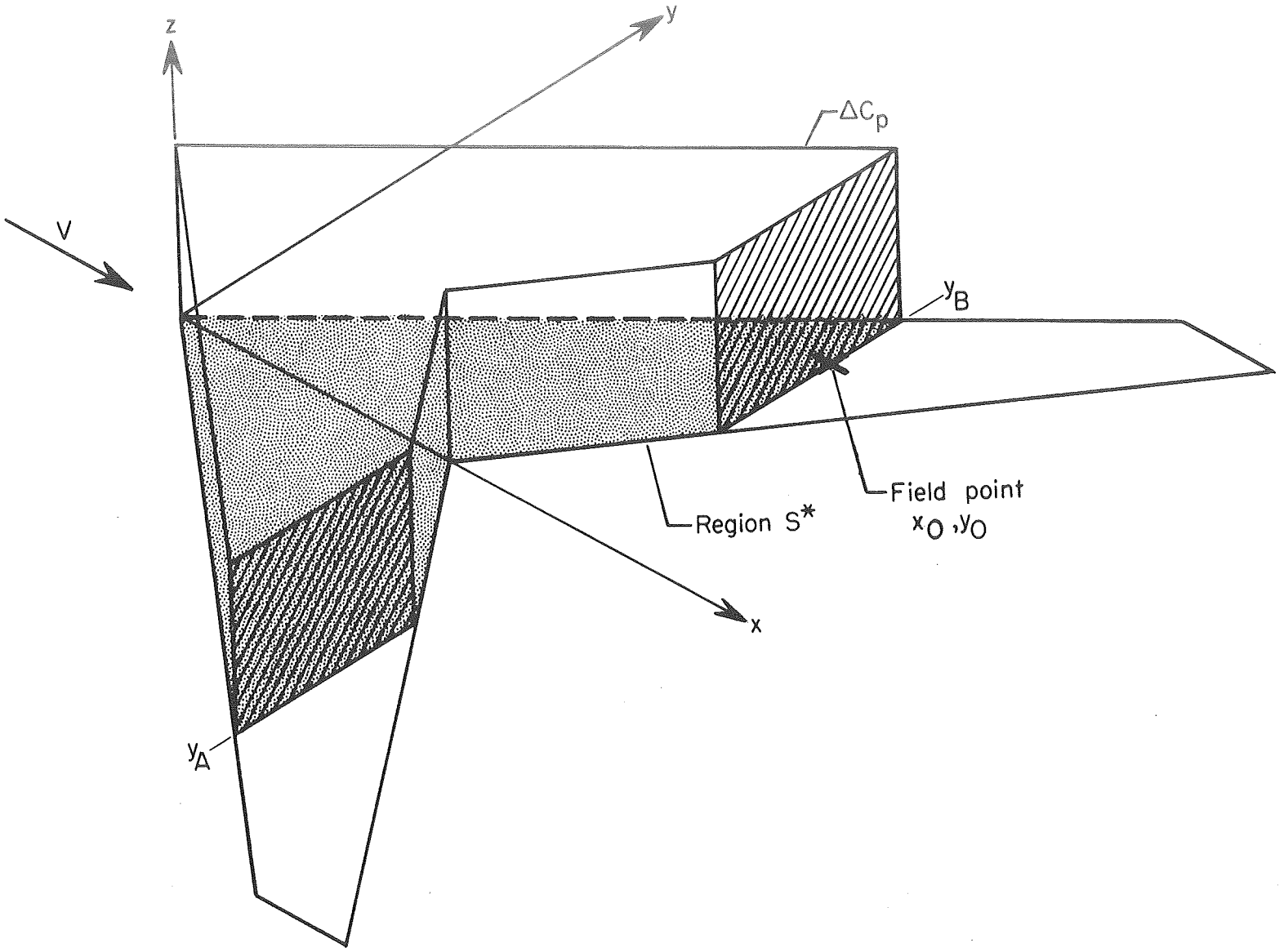

Figure 1.- Sketch of wing showing the partial wing loading on the region S*.

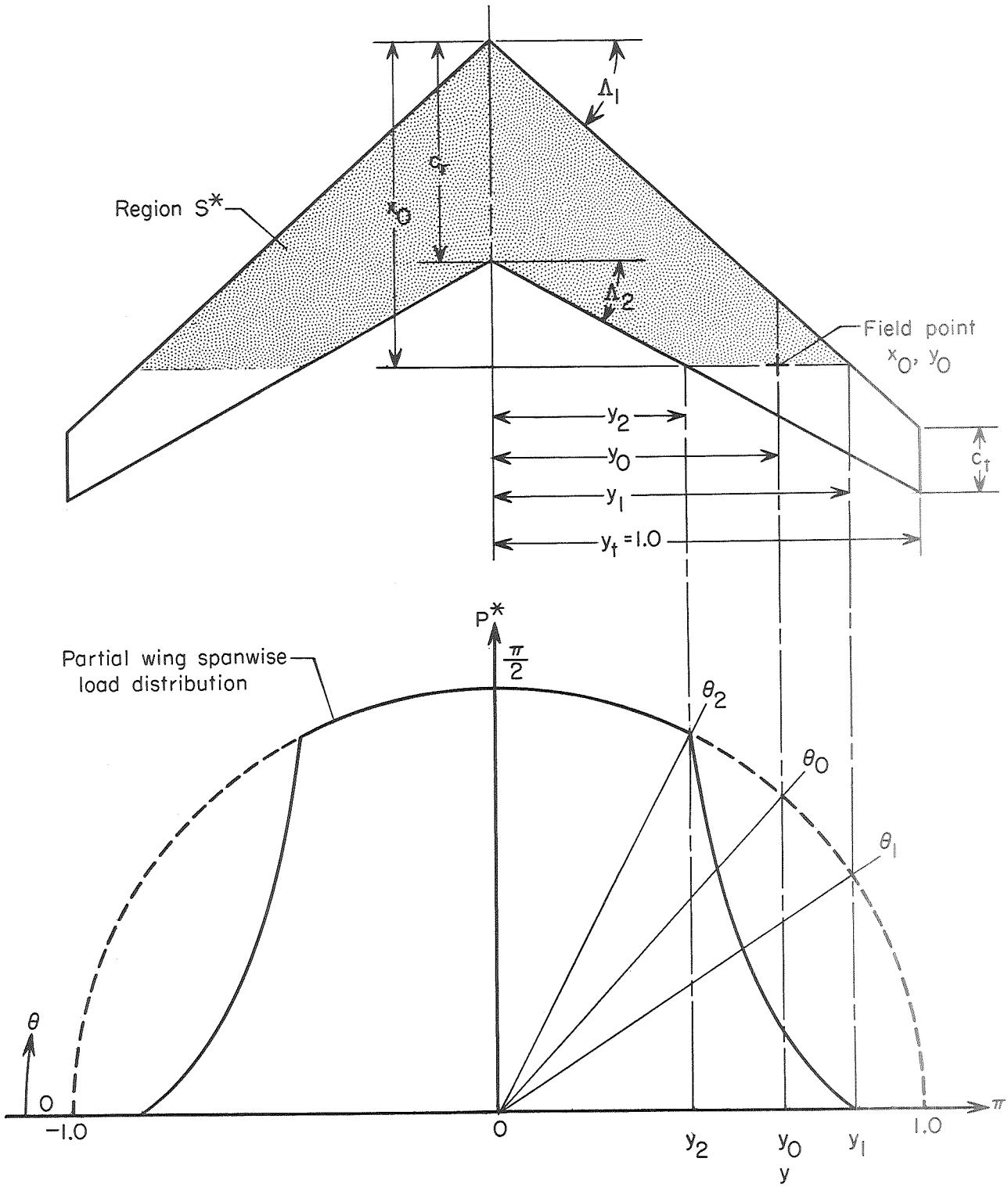

Figure 2.- Sketch showing wing planform geometry and the partial wing spanwise load distribution.

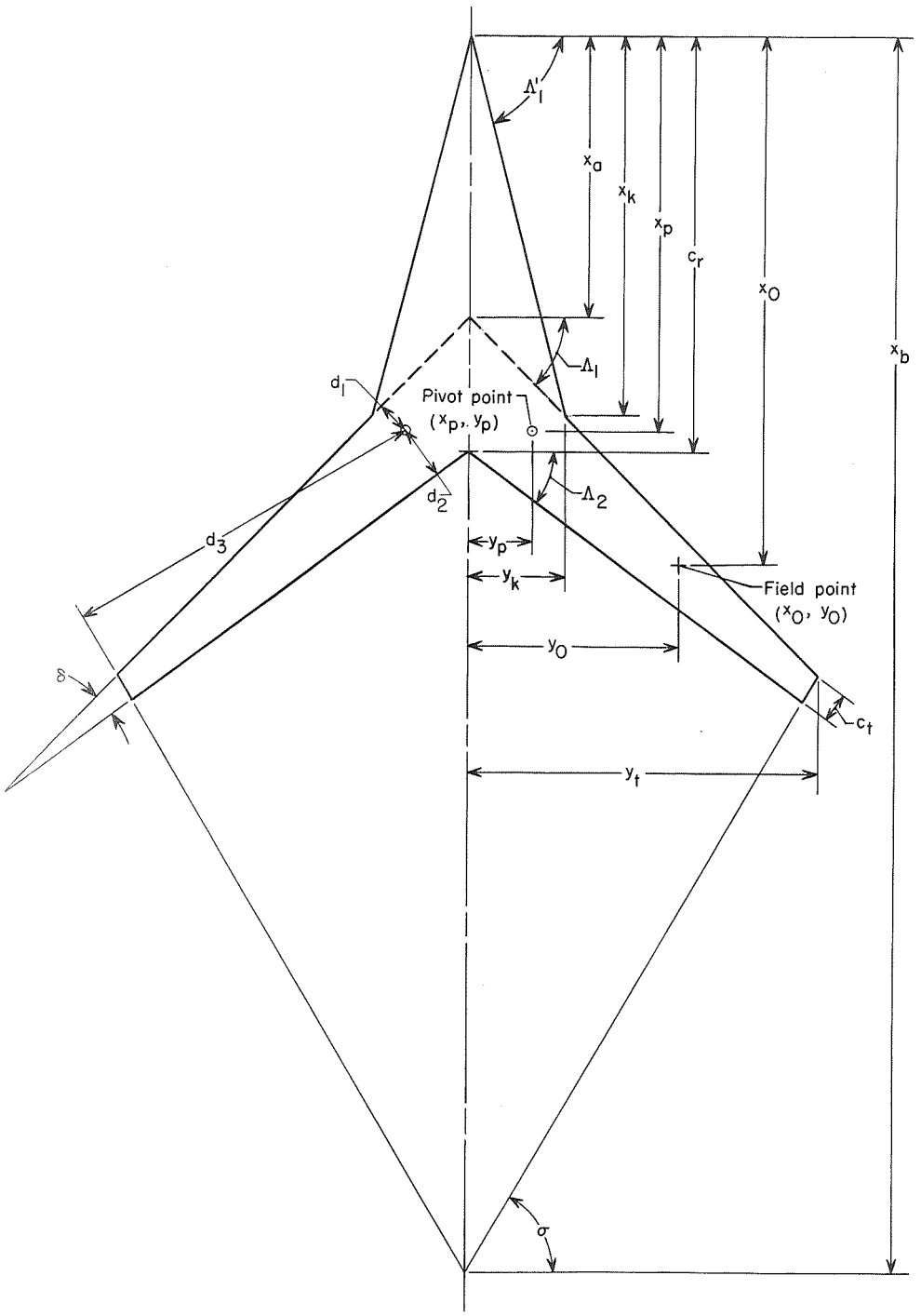

Figure 3.- Sketch showing geometry of variable-sweep wing.

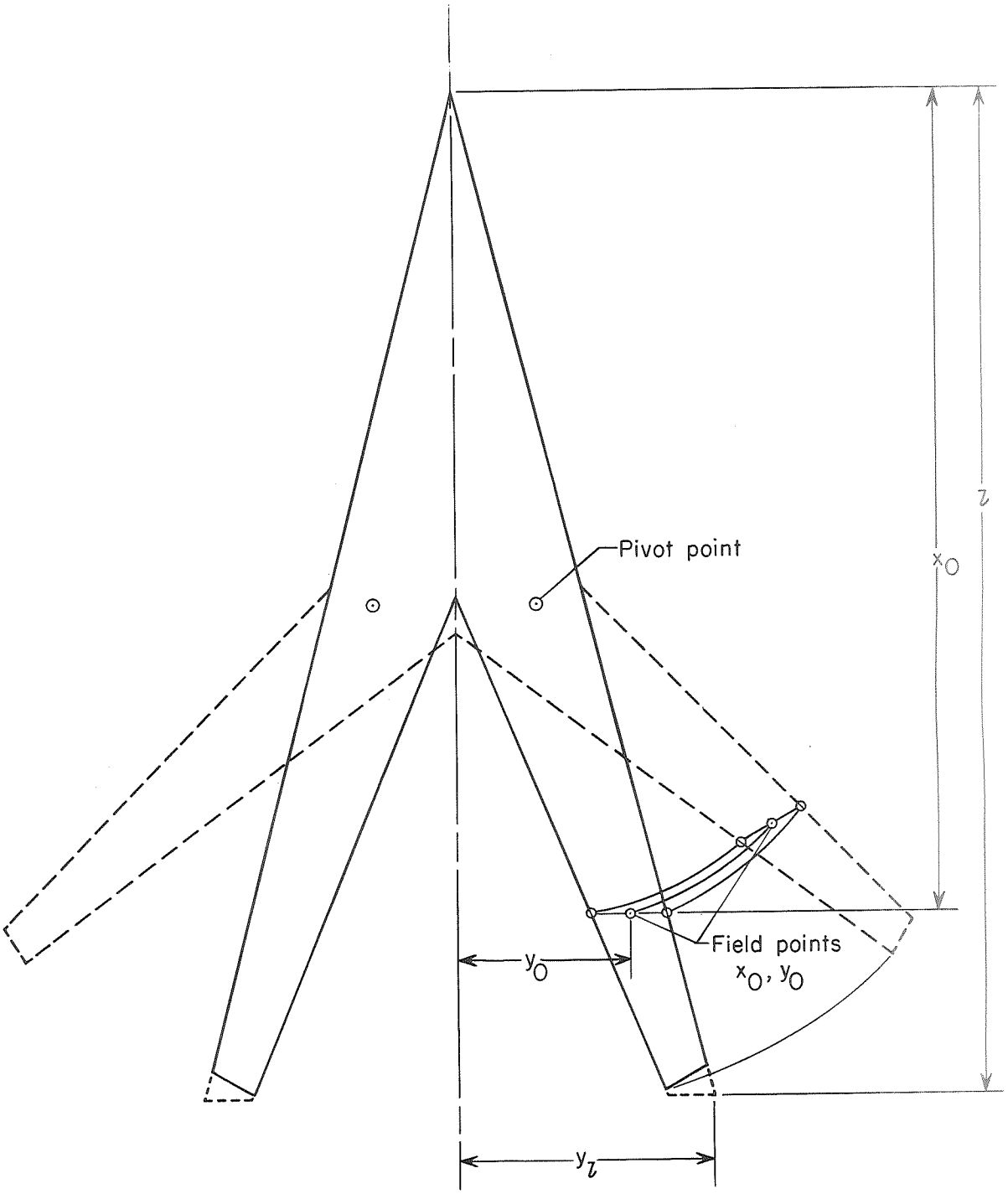

Figure 4.- Sketch showing changing location of field points with wing-sweep variation for variable-sweep wing mean line camber calculation.

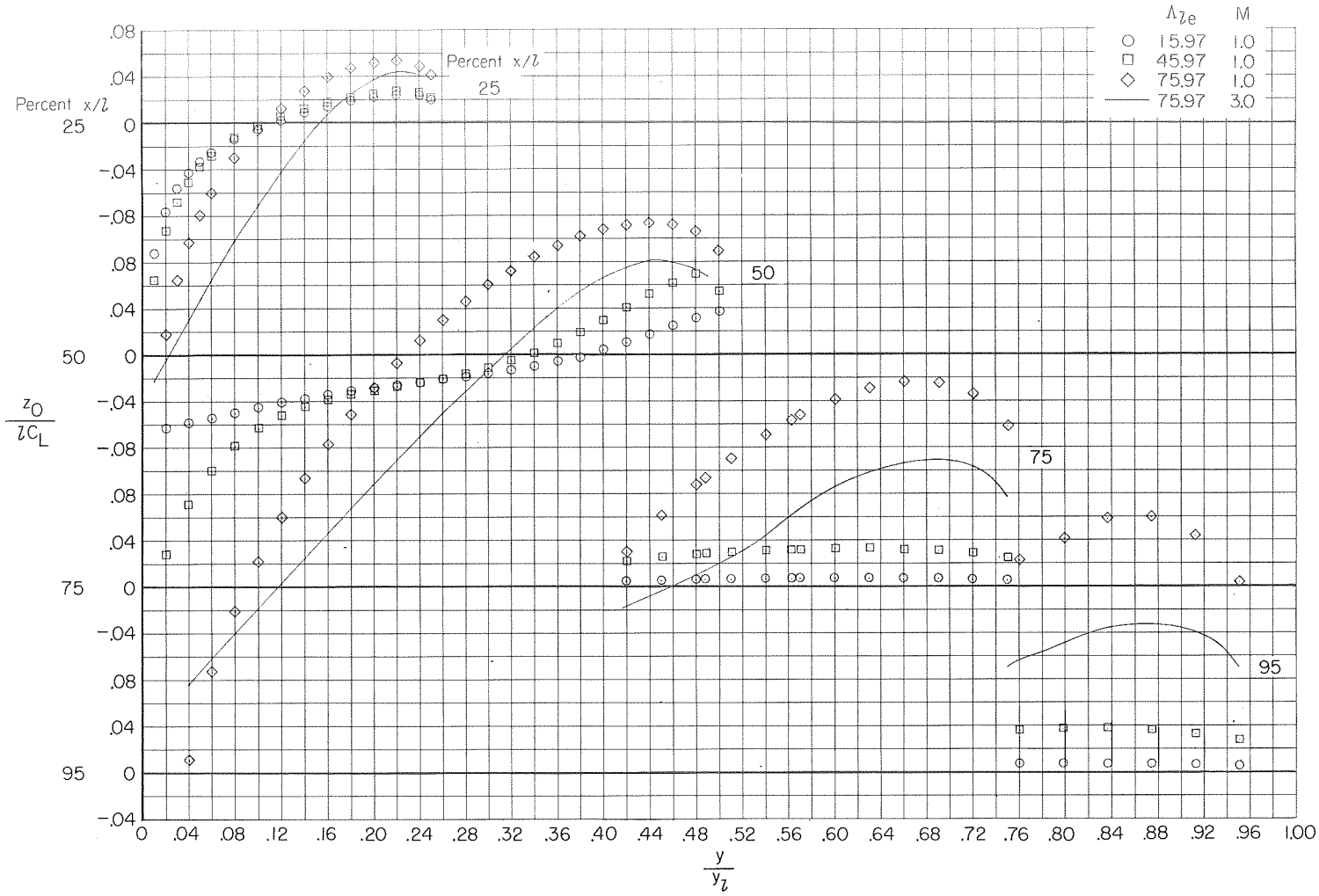

Figure 5.- Mean line camber for variable-sweep wing at three wing-sweep positions plotted as a function of field-point location on wing in fully sweptback position.

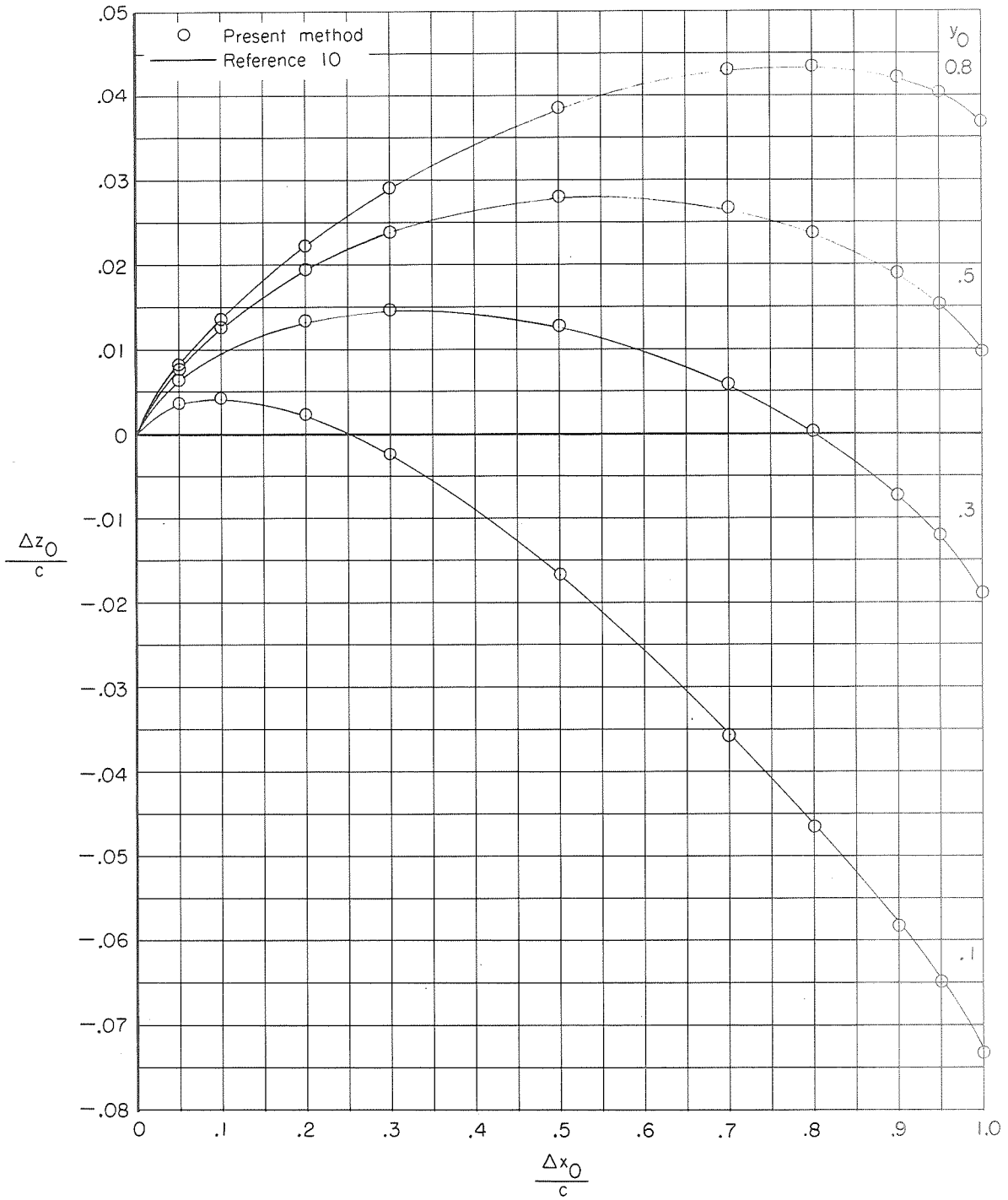

Figure 6.- Comparison of mean line camber calculated by present method and by method of reference 10 for a wing with $\Lambda_{c/4} = 40^{o}$, $A = 8$, and $\lambda = 0.3$ for $C_L = 0.514$.

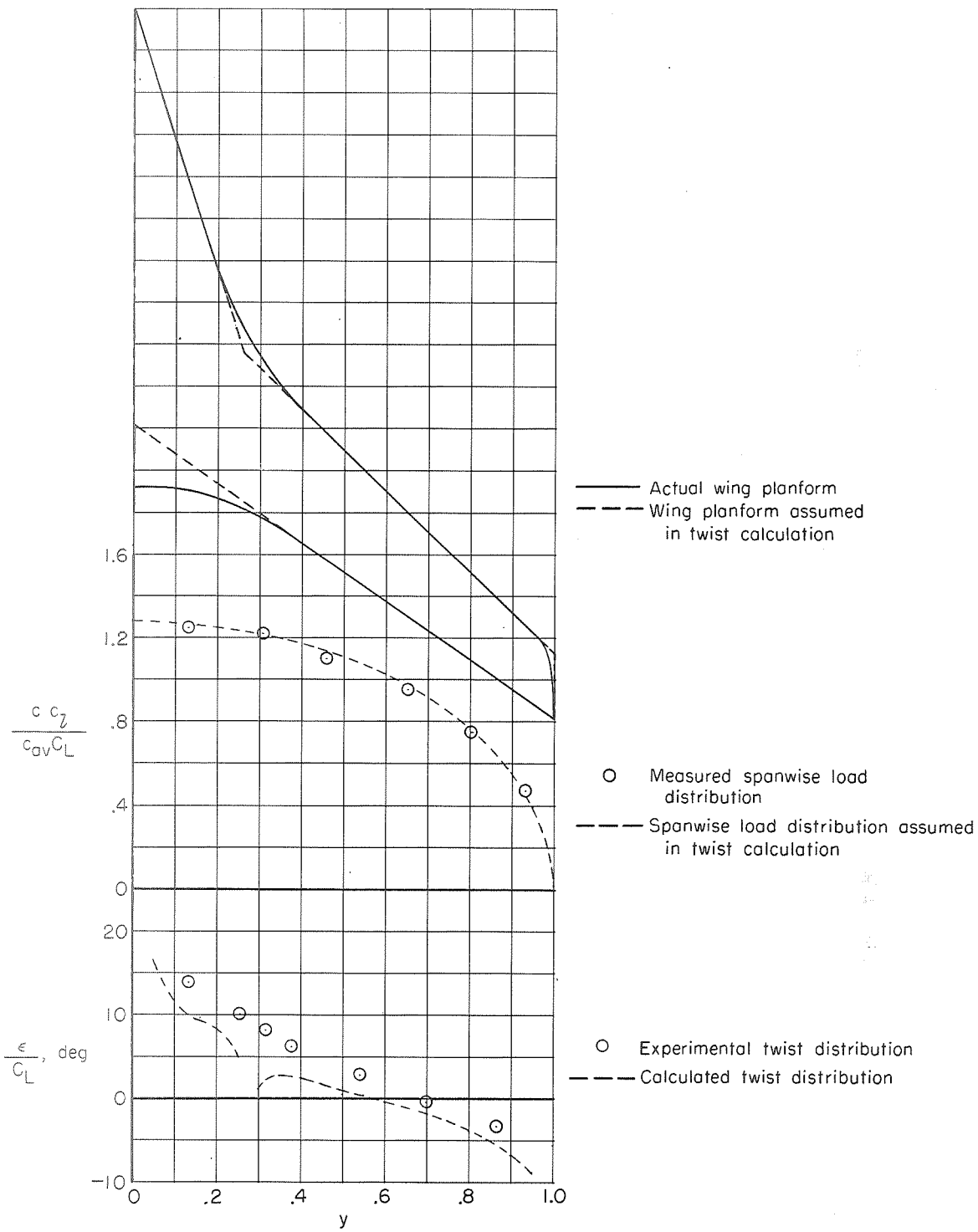

Figure 7.- Comparison of experimental and calculated twist distribution for a supercritical wing designed for near-sonic speeds.

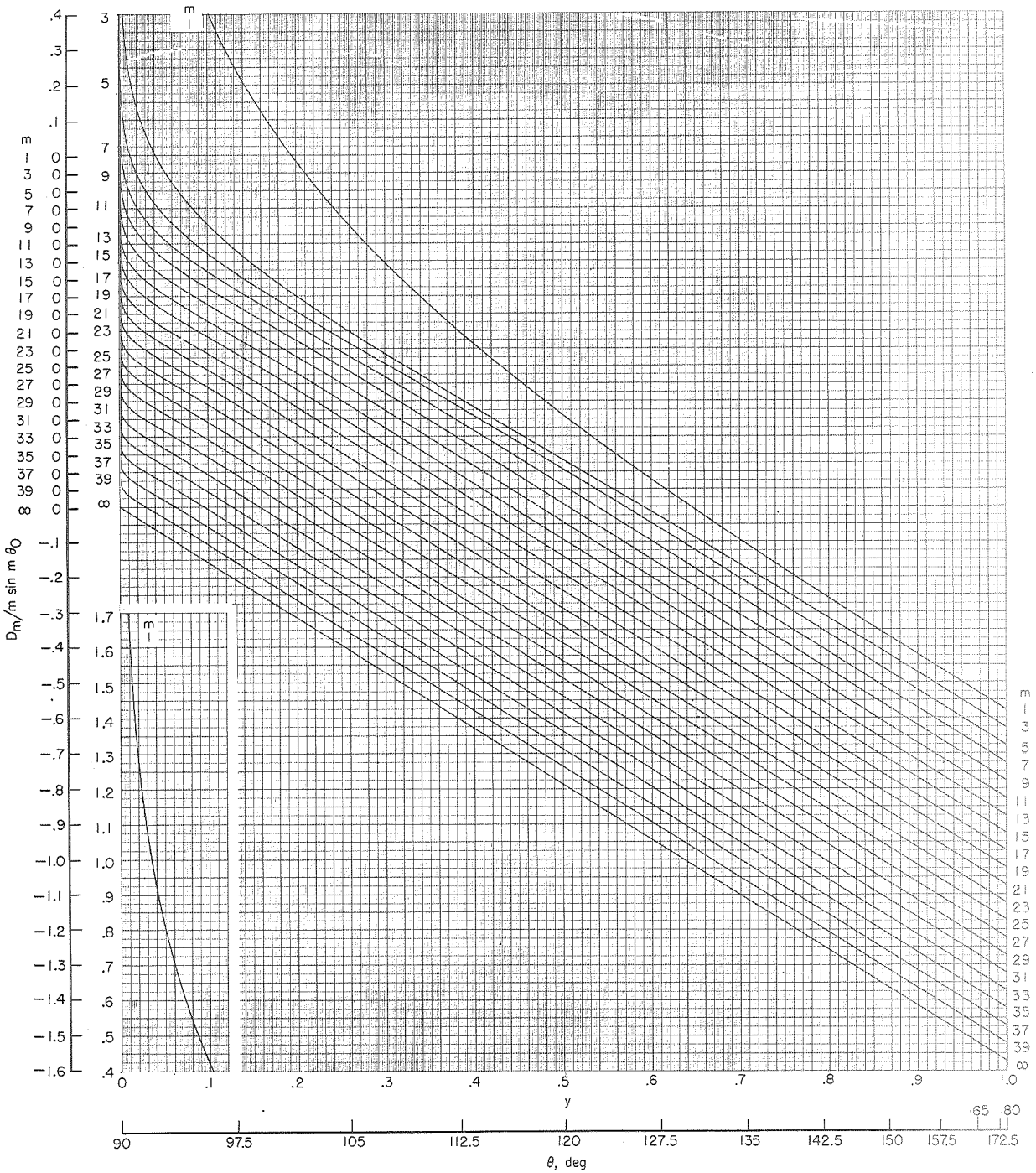

(a) $\theta_0 = 90^o$; $y_0 = 0$.

Figure 8.- $\frac{D_m}{m \sin m\theta_0}$ as a function of y for odd values of m from 1 to 39.

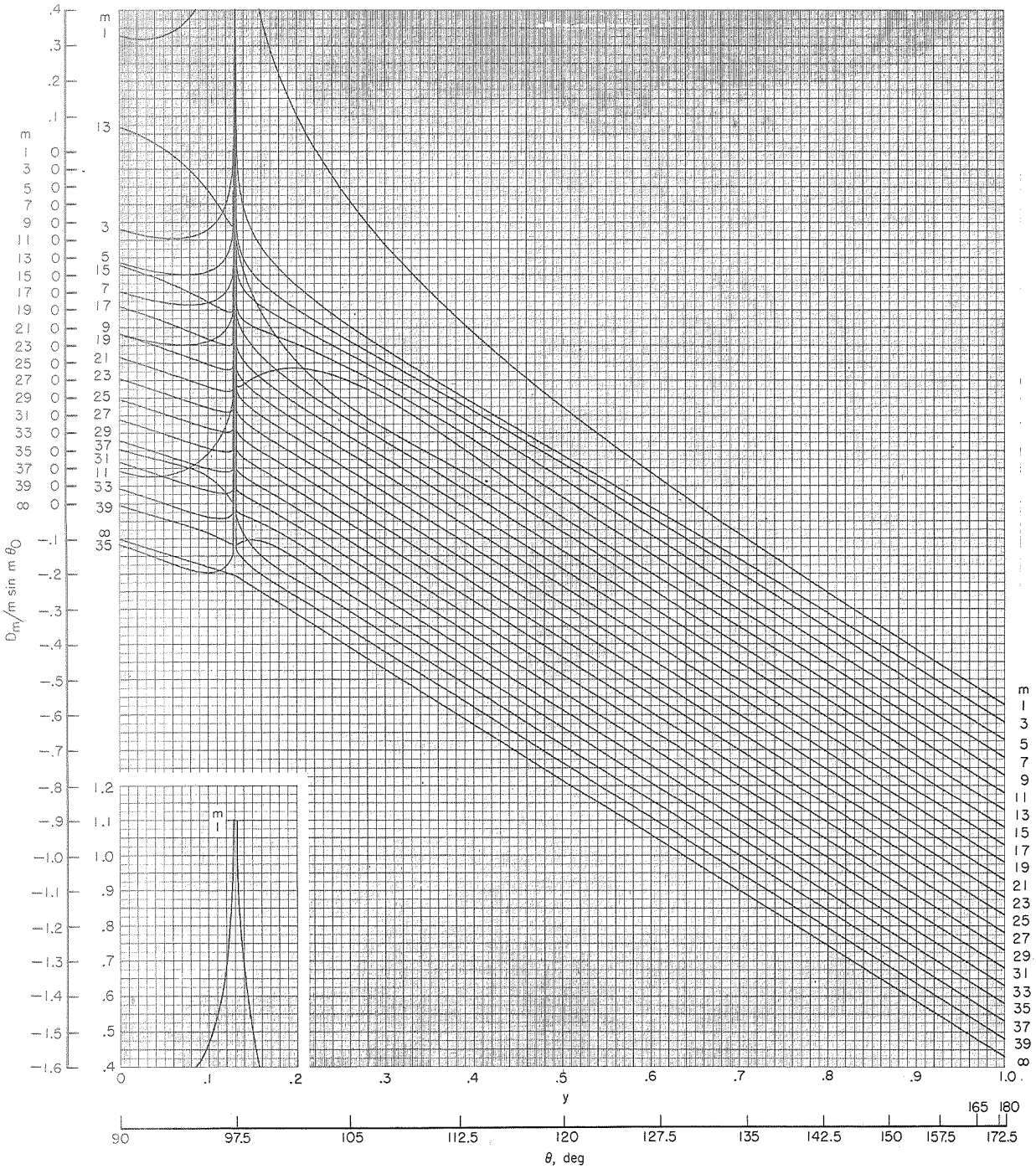

(b) $\theta_0 = 97.5^{\circ}$; $y_0 = 0.13053$.

Figure 8.- Continued.

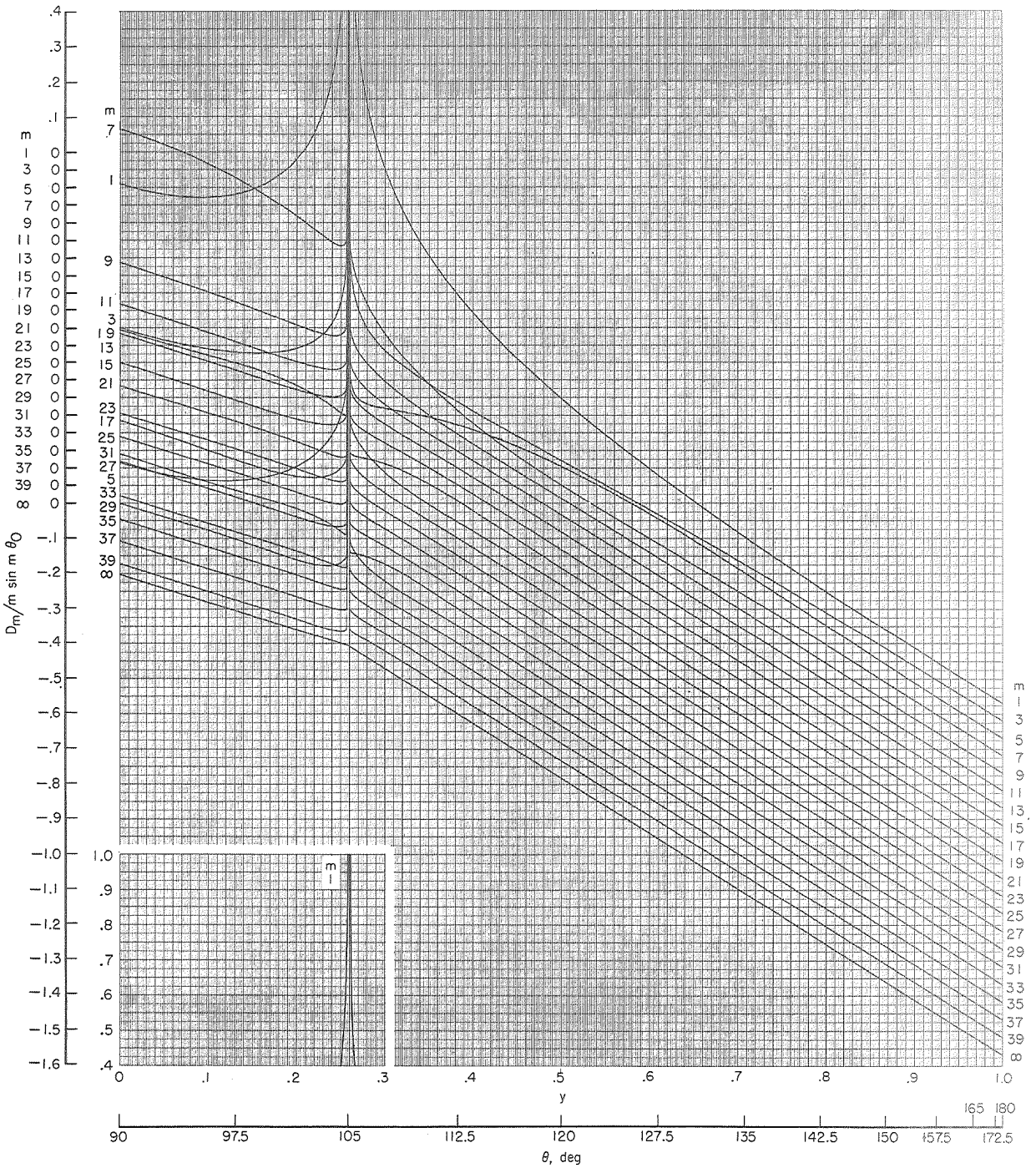

(c) $\theta_0 = 105^o$; $y_0 = 0.25882$.

Figure 8.- Continued.

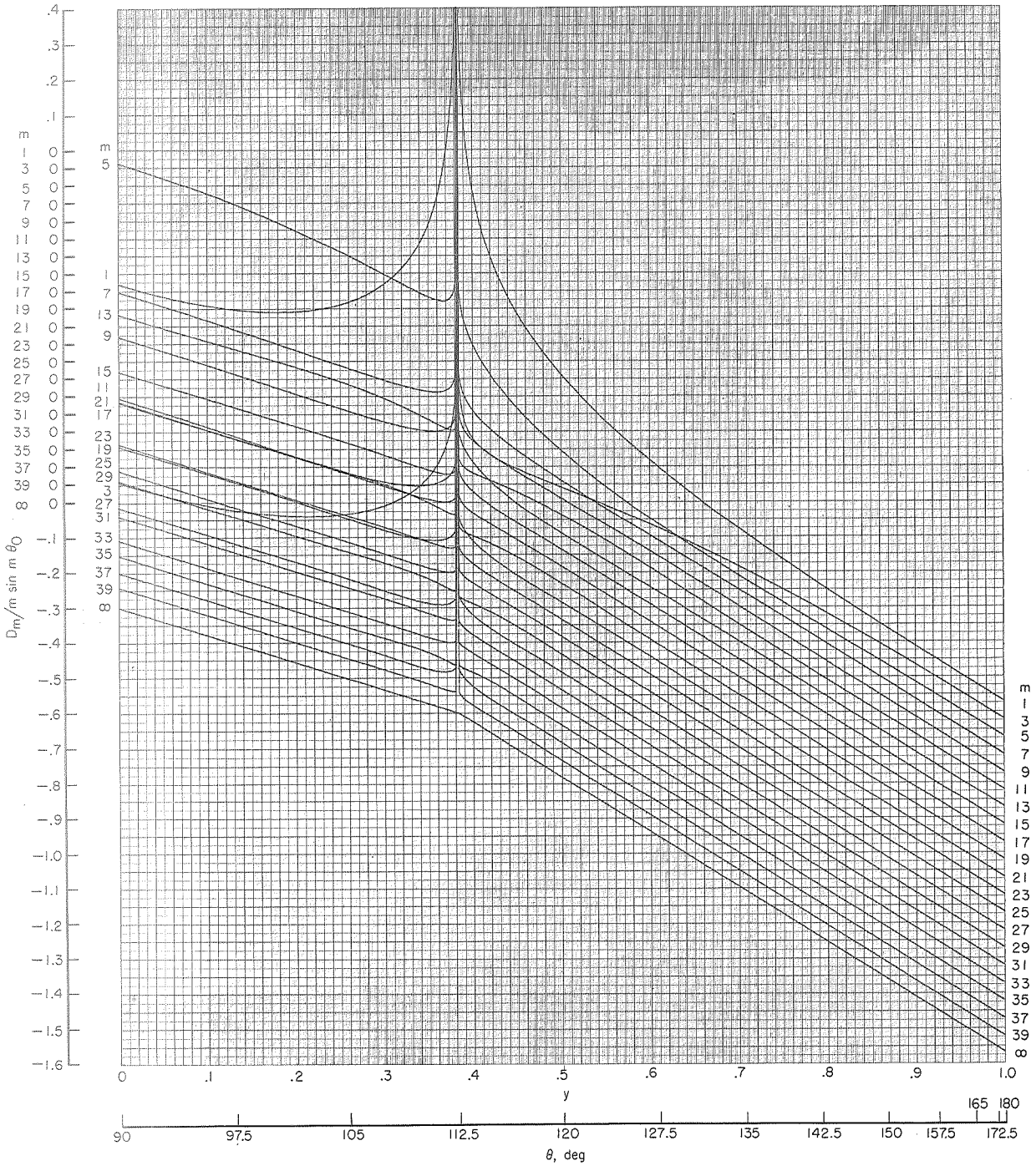

(d) $\theta_0 = 112.5^{\circ}$; $y_0 = 0.38268$.

Figure 8.- Continued.

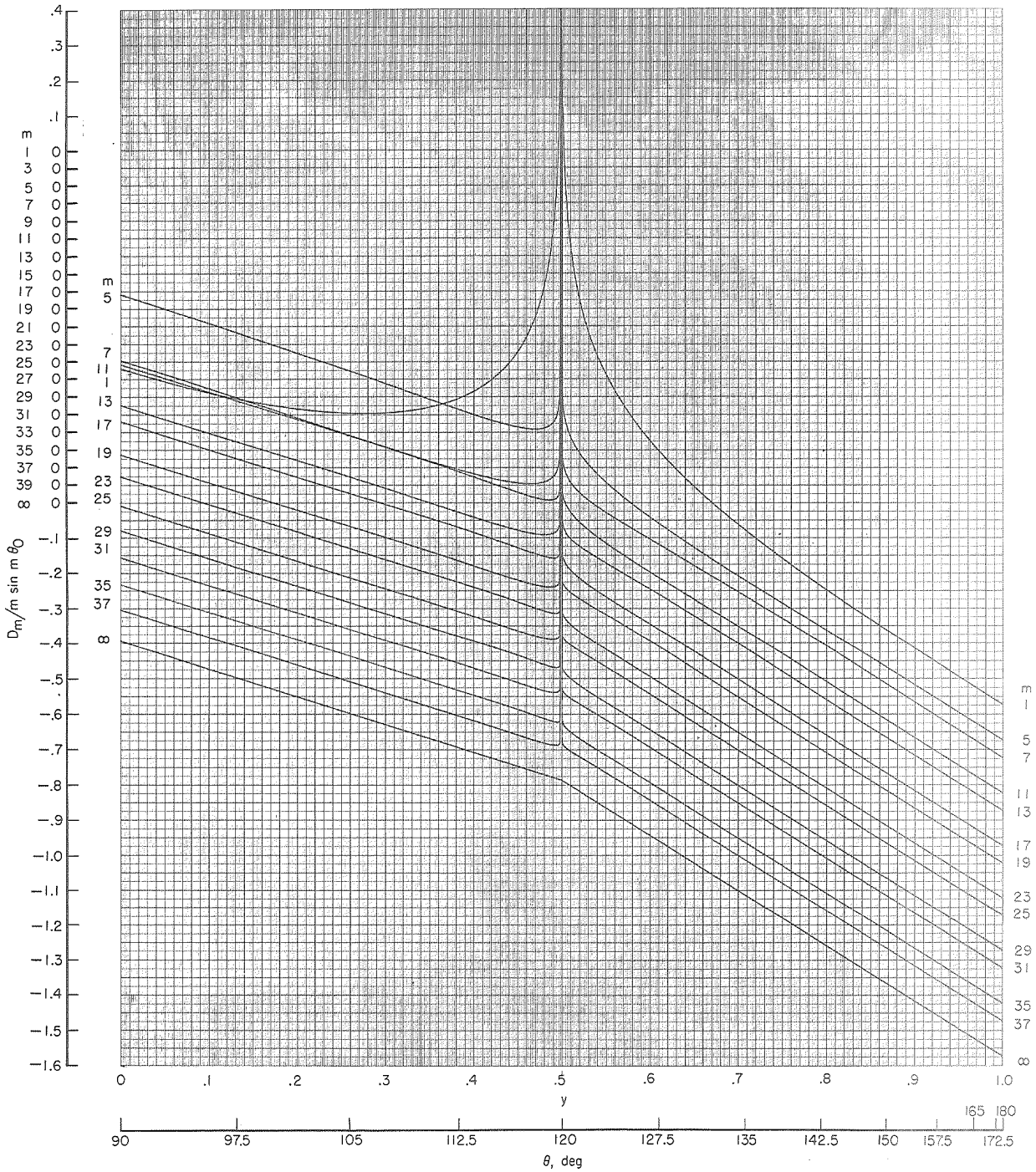

(e) $\theta_0 = 120^{\circ}$; $y_0 = 0.50000$.

Figure 8.- Continued.

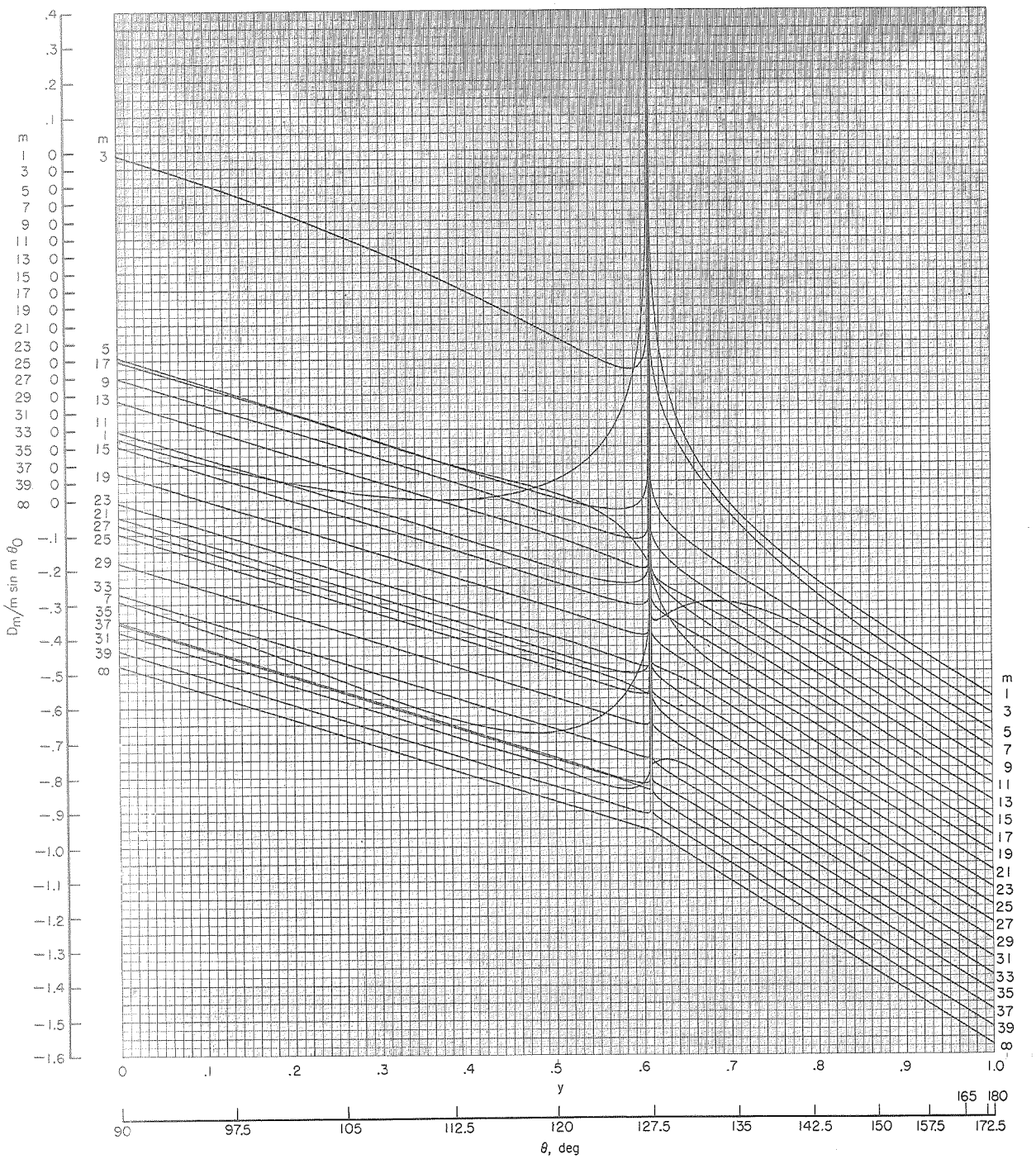

(f) $\theta_0 = 127.5^{\circ}$; $y_0 = 0.60876$.

Figure 8.- Continued.

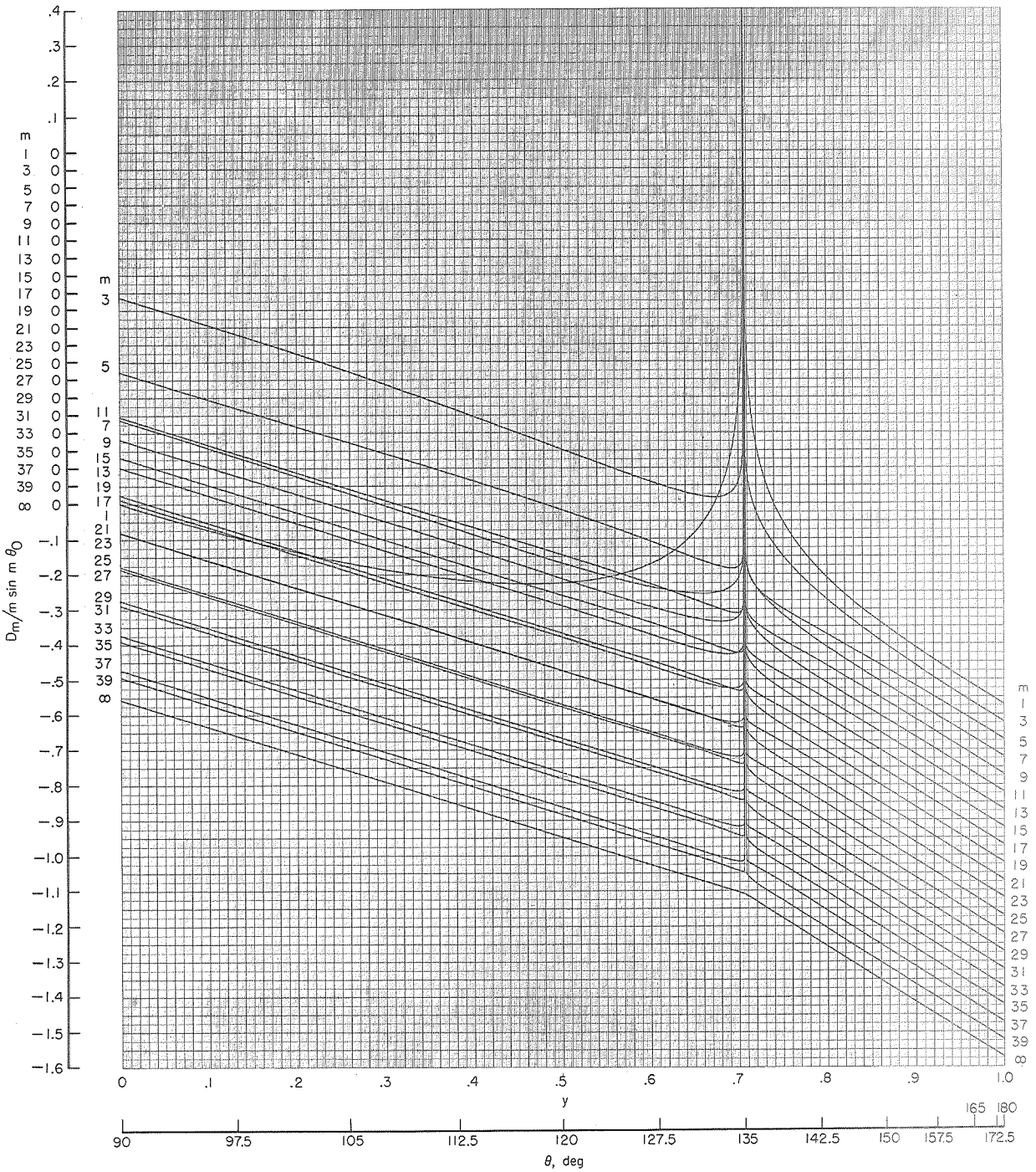

(g) $\theta_0 = 135^{\circ}$; $y_0 = 0.70711$.

Figure 8.- Continued.

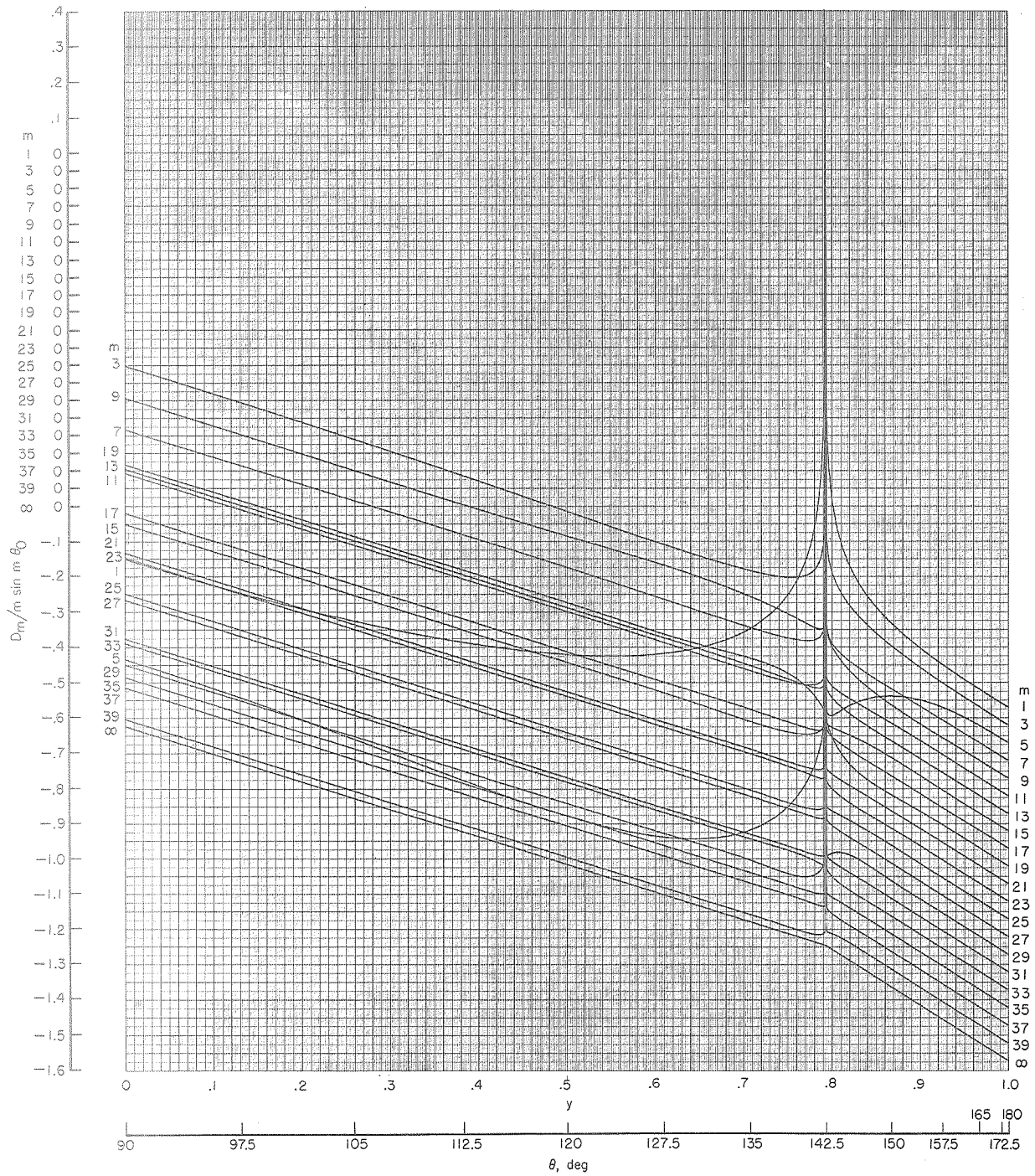

(h) $\theta_0 = 142.5^{\circ}$; $y_0 = 0.79335$.

Figure 8.- Continued.

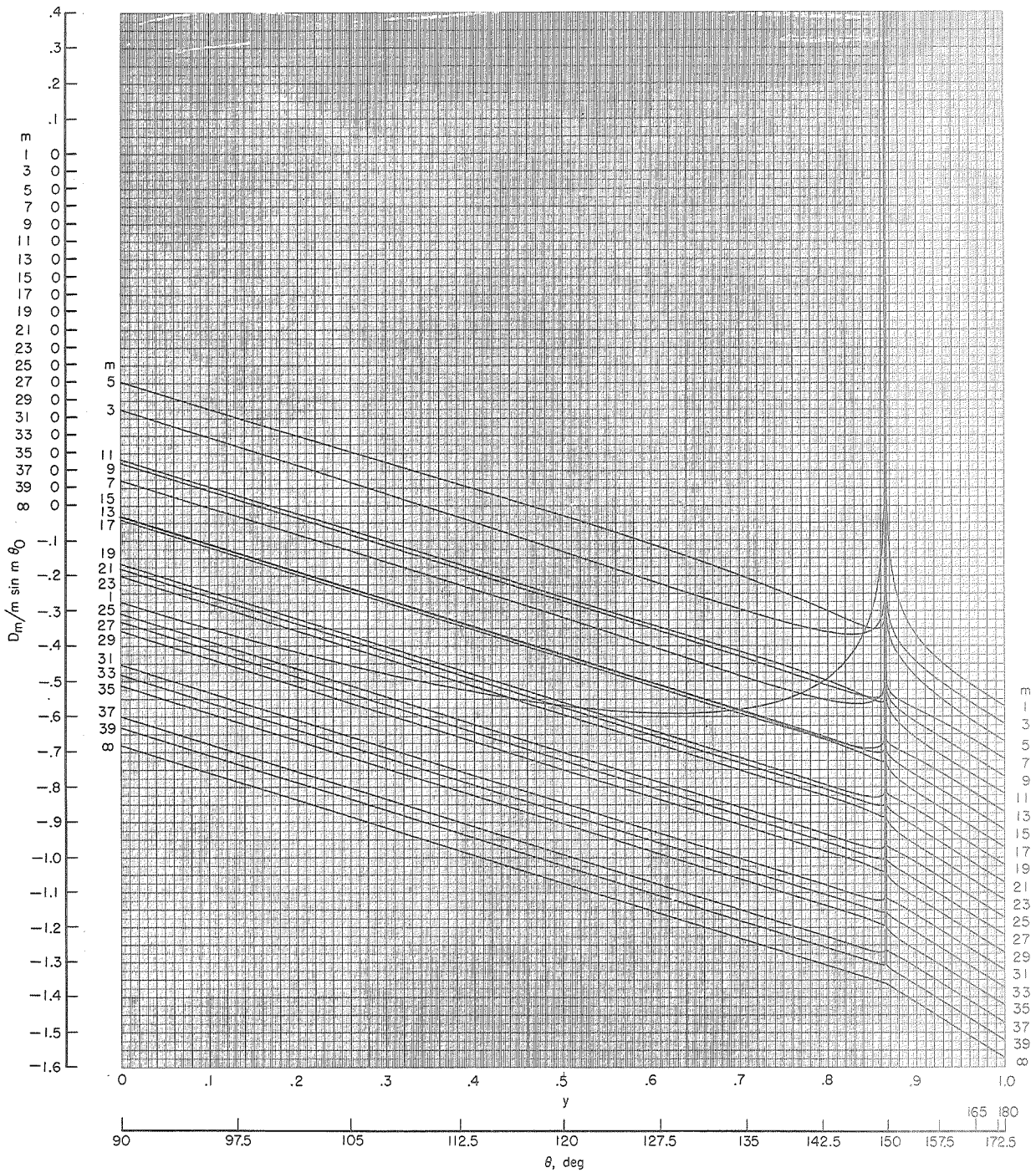

(i) $\theta_0 = 150^{\circ}$; $y_0 = 0.86603$.

Figure 8.- Continued.

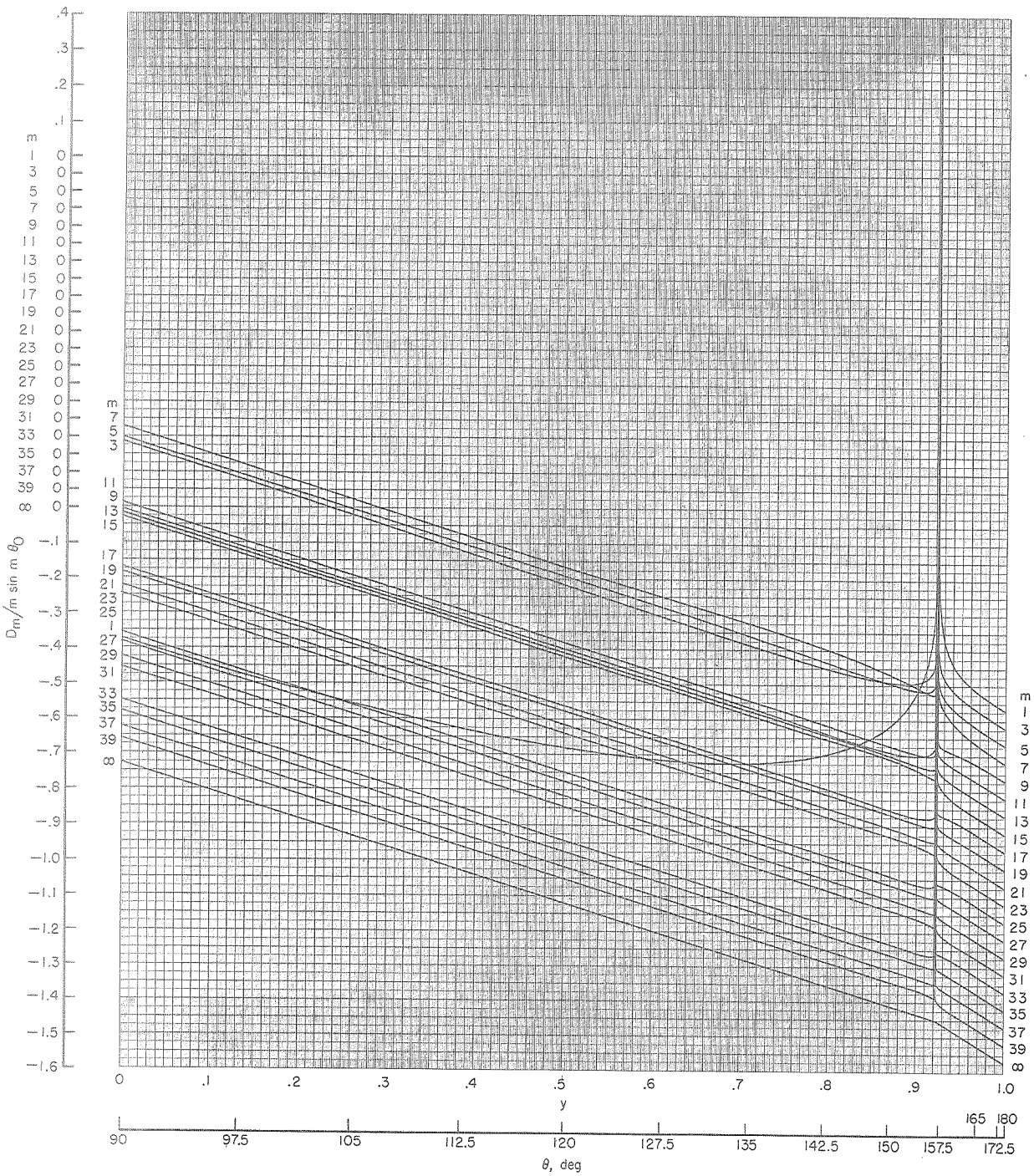

(j) $\theta_0 = 157.5^{\circ}$; $y_0 = 0.92388$.

Figure 8.- Continued.

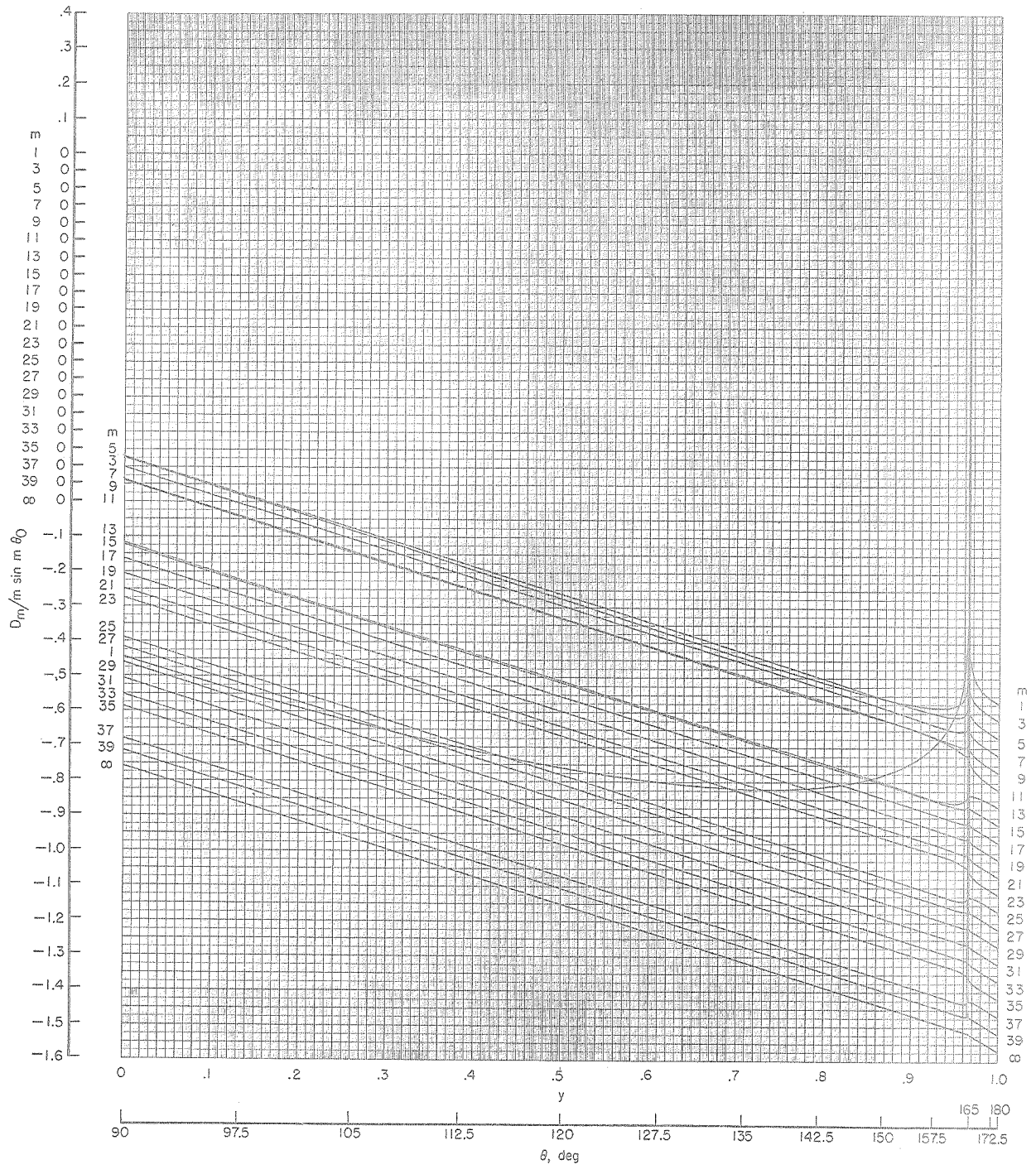

(k) $\theta_0 = 165^{\circ}$; $y_0 = 0.96593$.

Figure 8.- Continued.

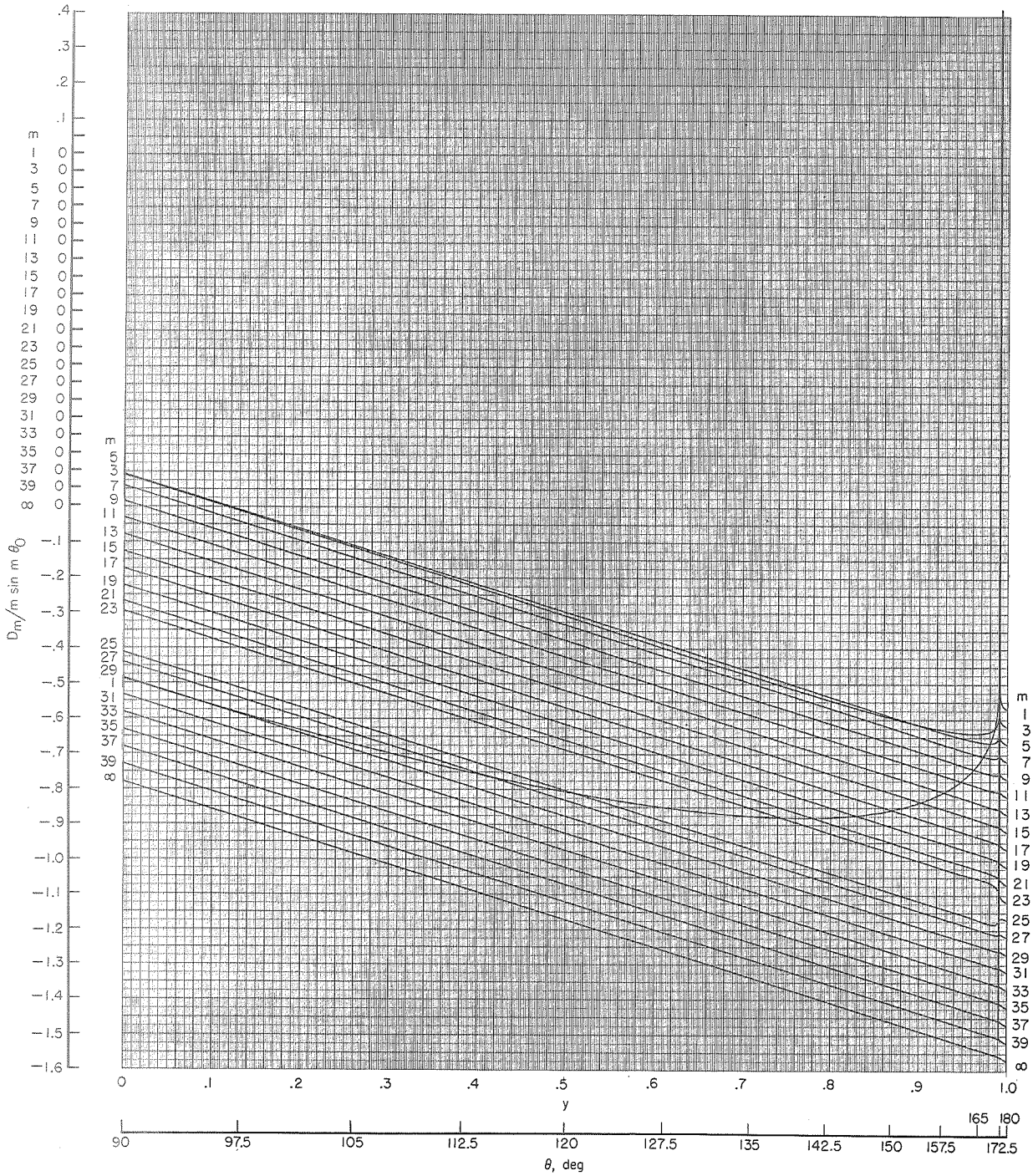

(*l*) $\theta_0 = 172.5^{\circ}$; $y_0 = 0.99144$.

Figure 8.- Concluded.

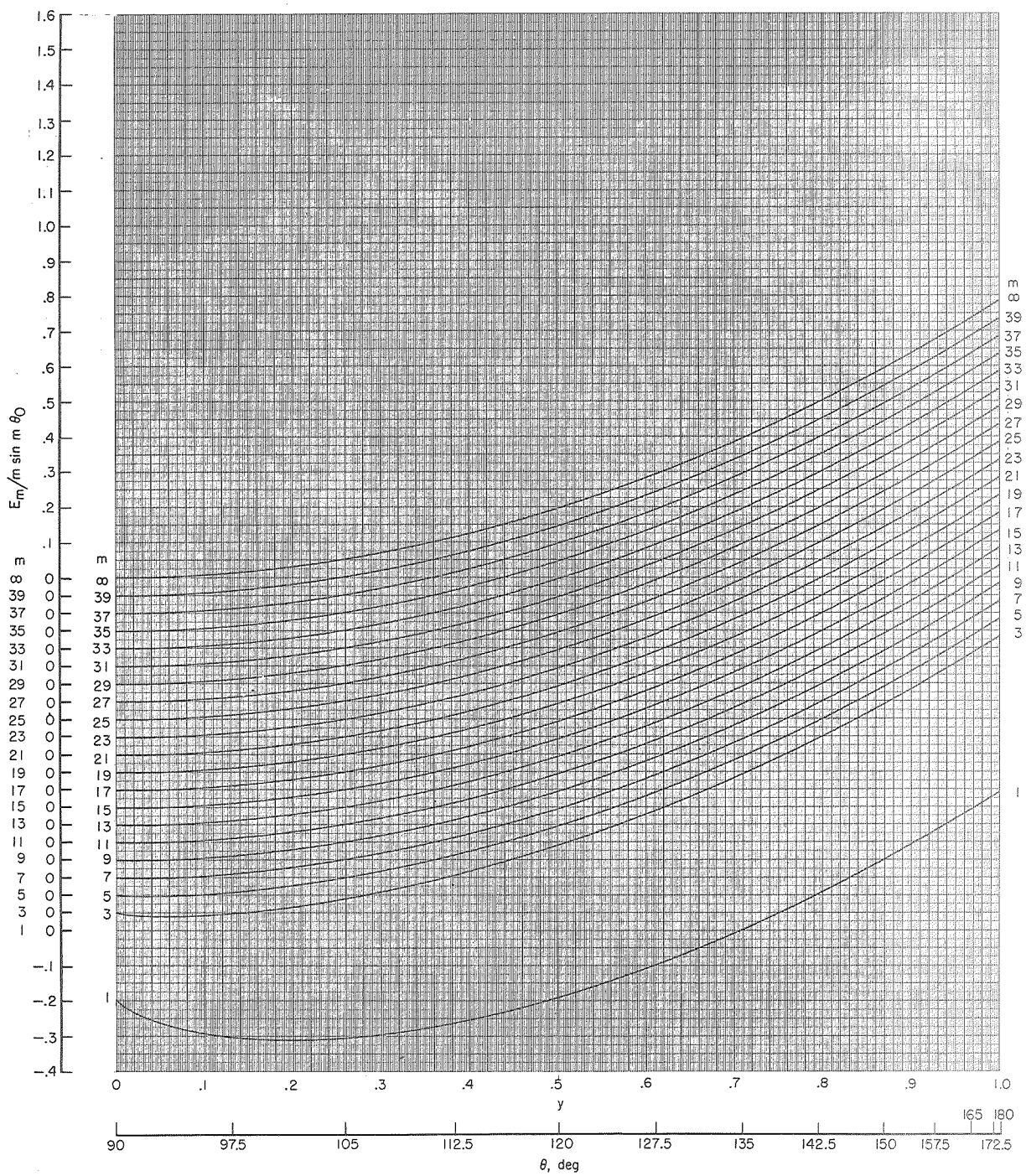

(a) $\theta_0 = 90^o$; $y_0 = 0$.

Figure 9.- $\frac{E_m}{m \sin m\theta_0}$ as a function of y for odd values of m from 1 to 39.

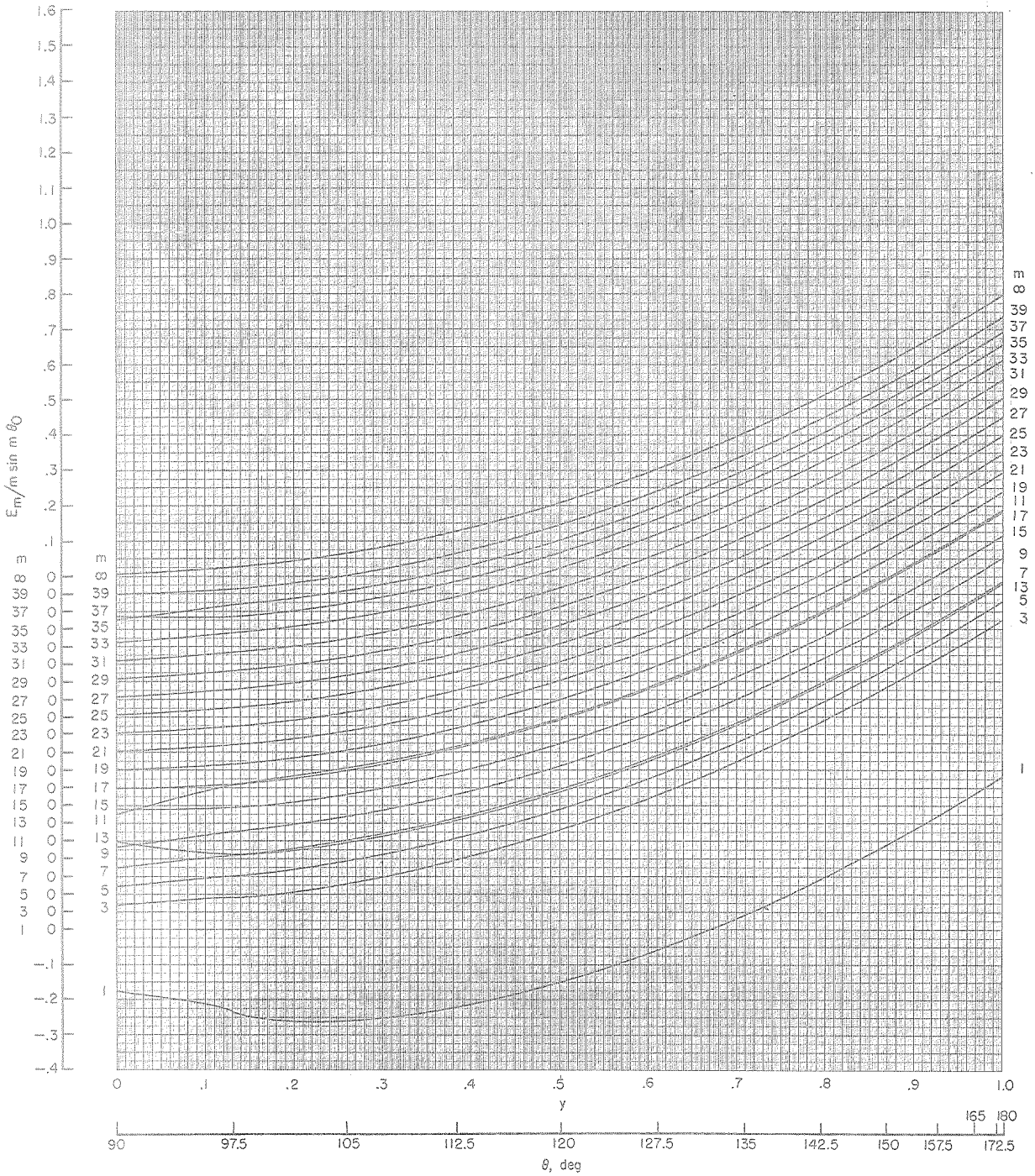

(b) $\theta_0 = 97.5^{\circ}$; $y_0 = 0.13053$.

Figure 9.- Continued.

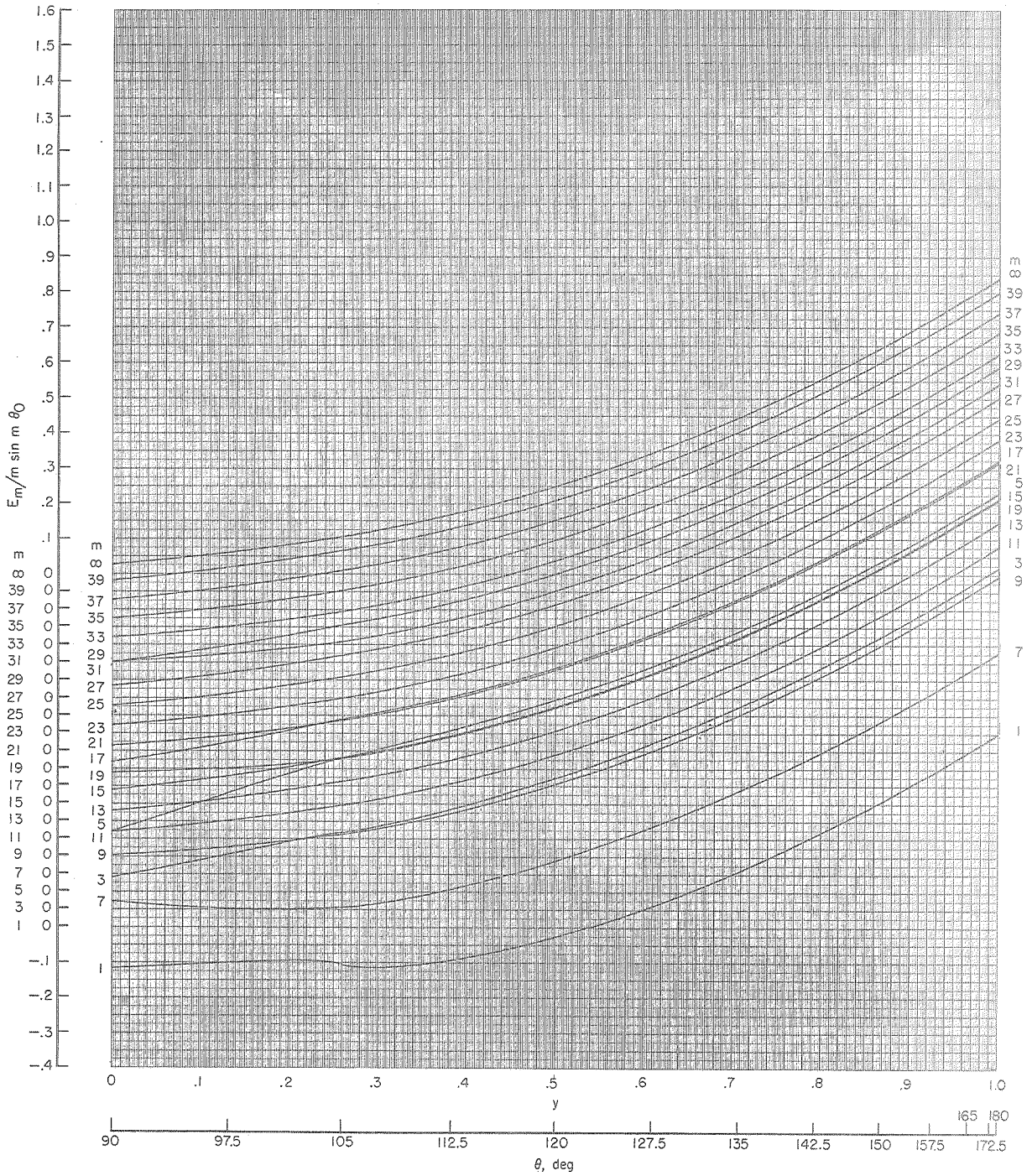

(c) $\theta_0 = 105^\circ$; $y_0 = 0.25882$.

Figure 9.- Continued.

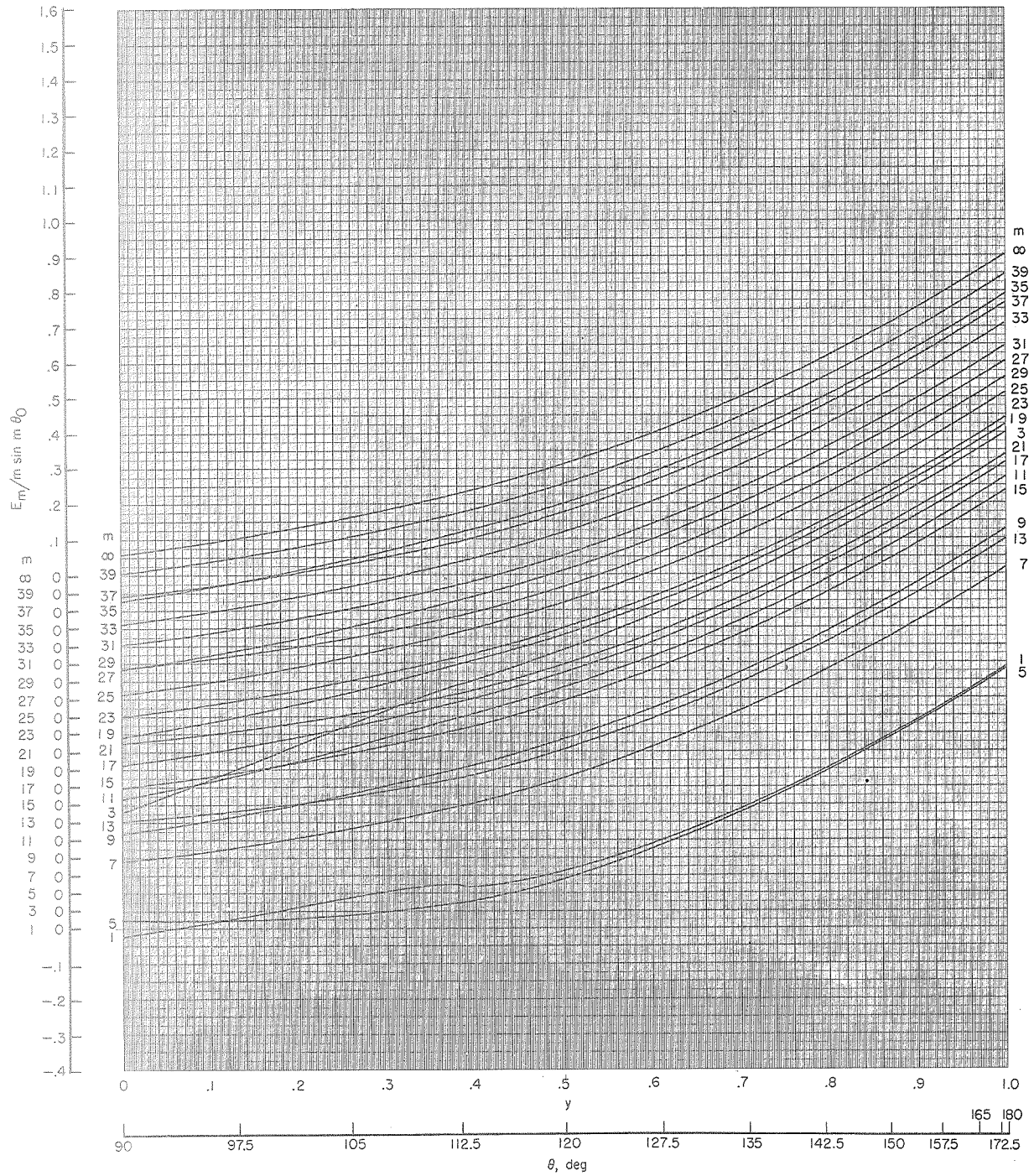

(d) $\theta_0 = 112.5^o$; $y_0 = 0.38268$.

Figure 9.- Continued.

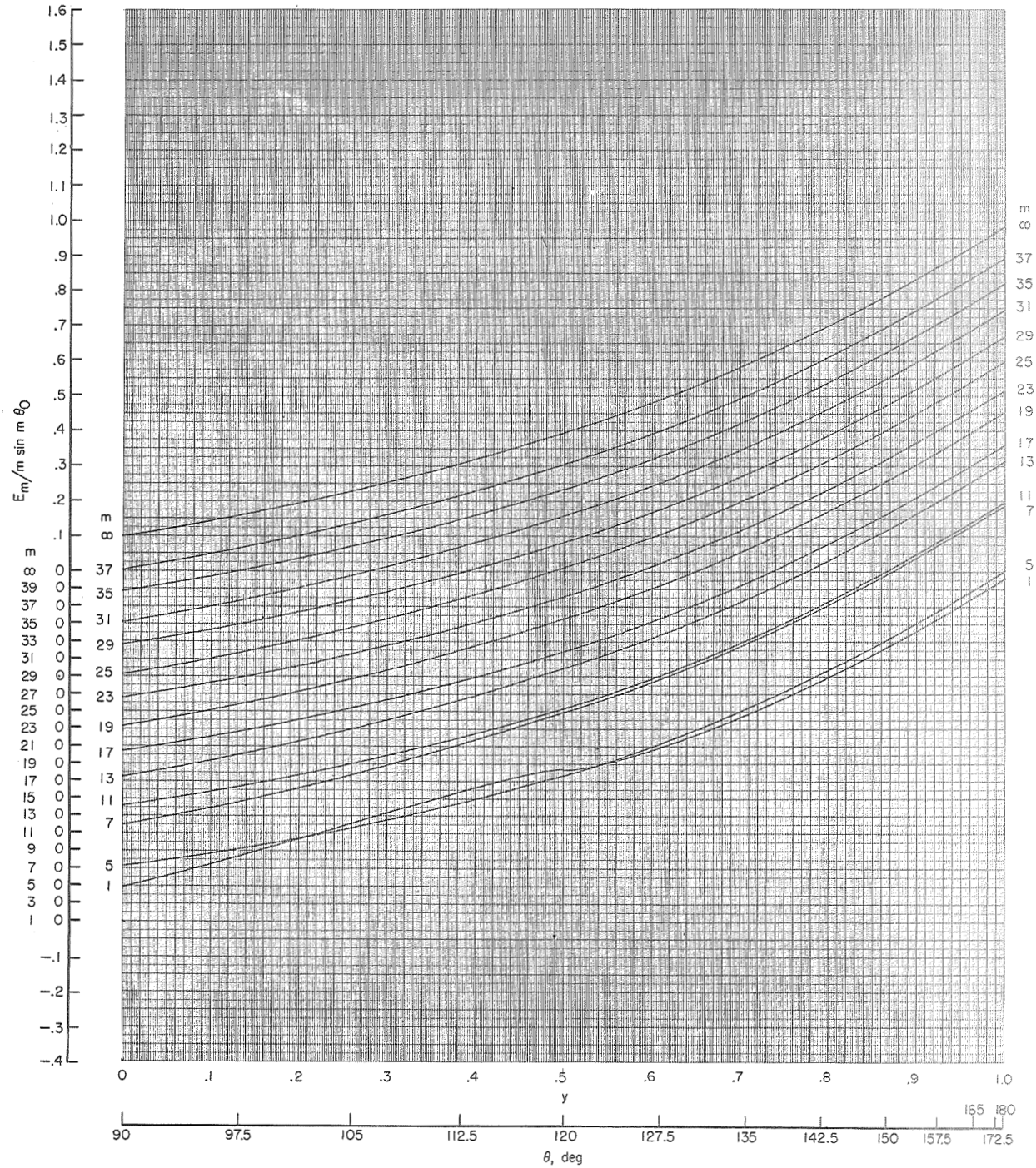

(e) $\theta_0 = 120^\circ$; $y_0 = 0.50000$.

Figure 9.- Continued.

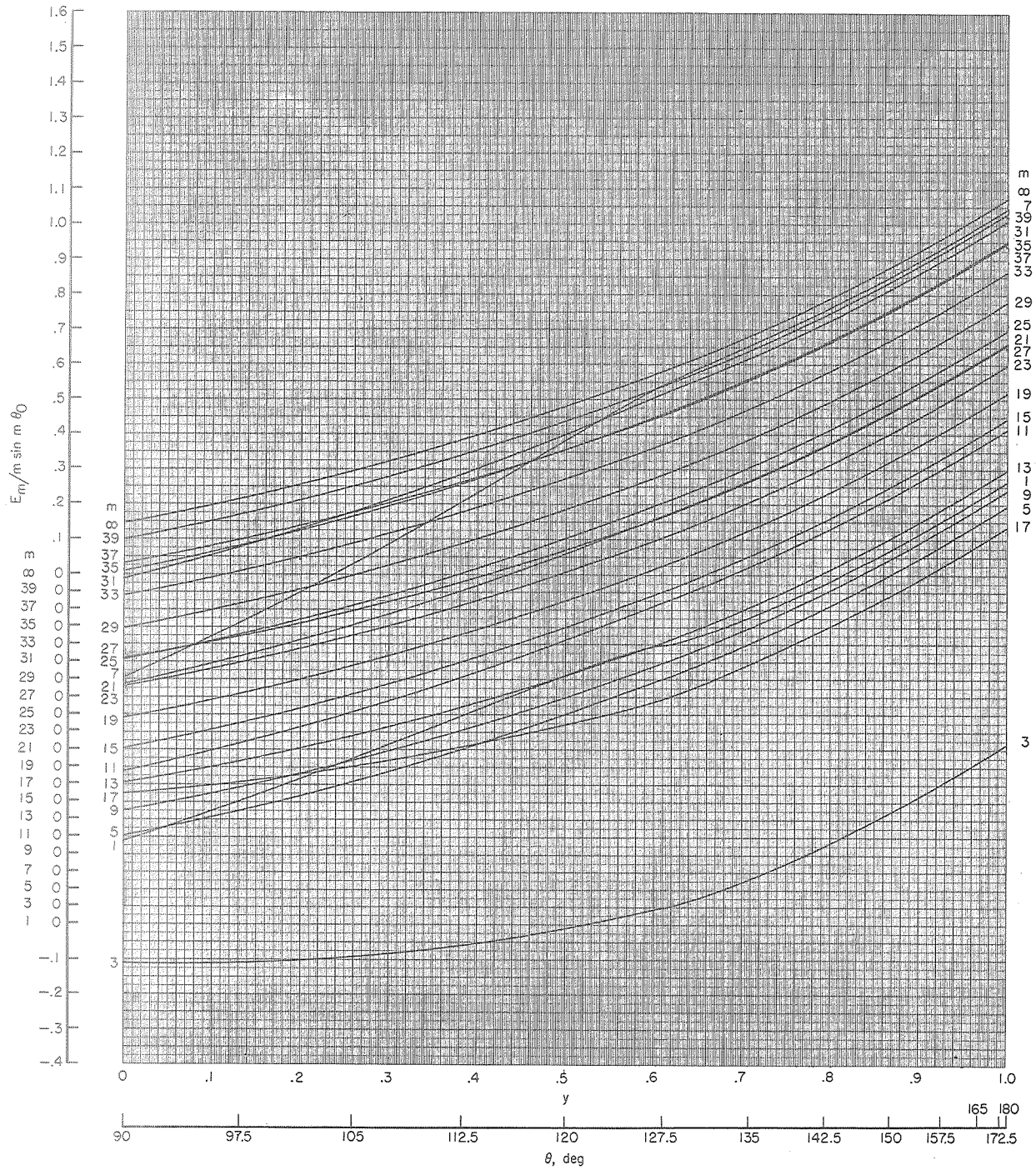

(f) $\theta_0 = 127.5^{\circ}$; $y_0 = 0.60876$.

Figure 9.- Continued.

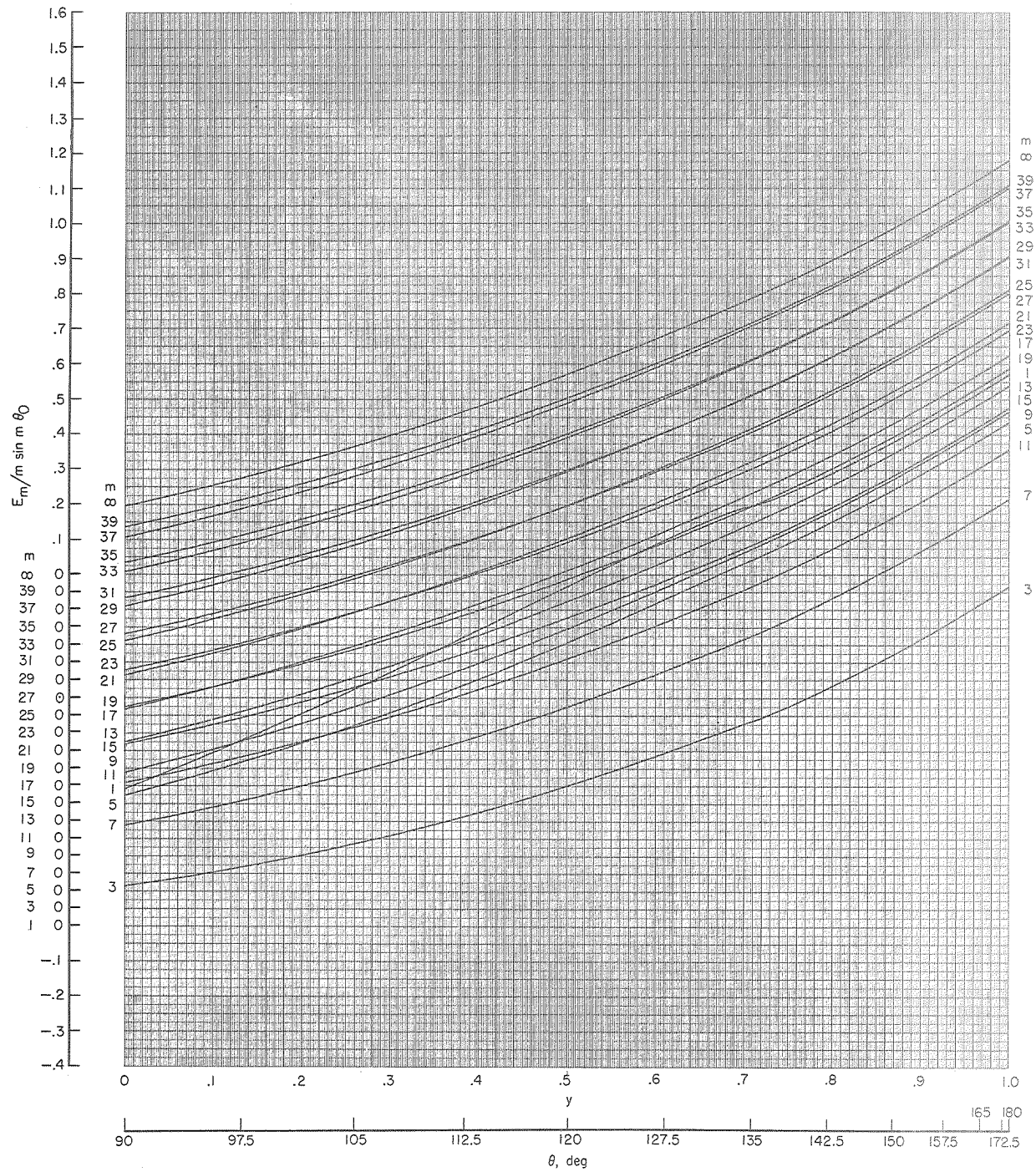

(g) $\theta_0 = 135^{\circ}$; $y_0 = 0.70711$.

Figure 9.- Continued.

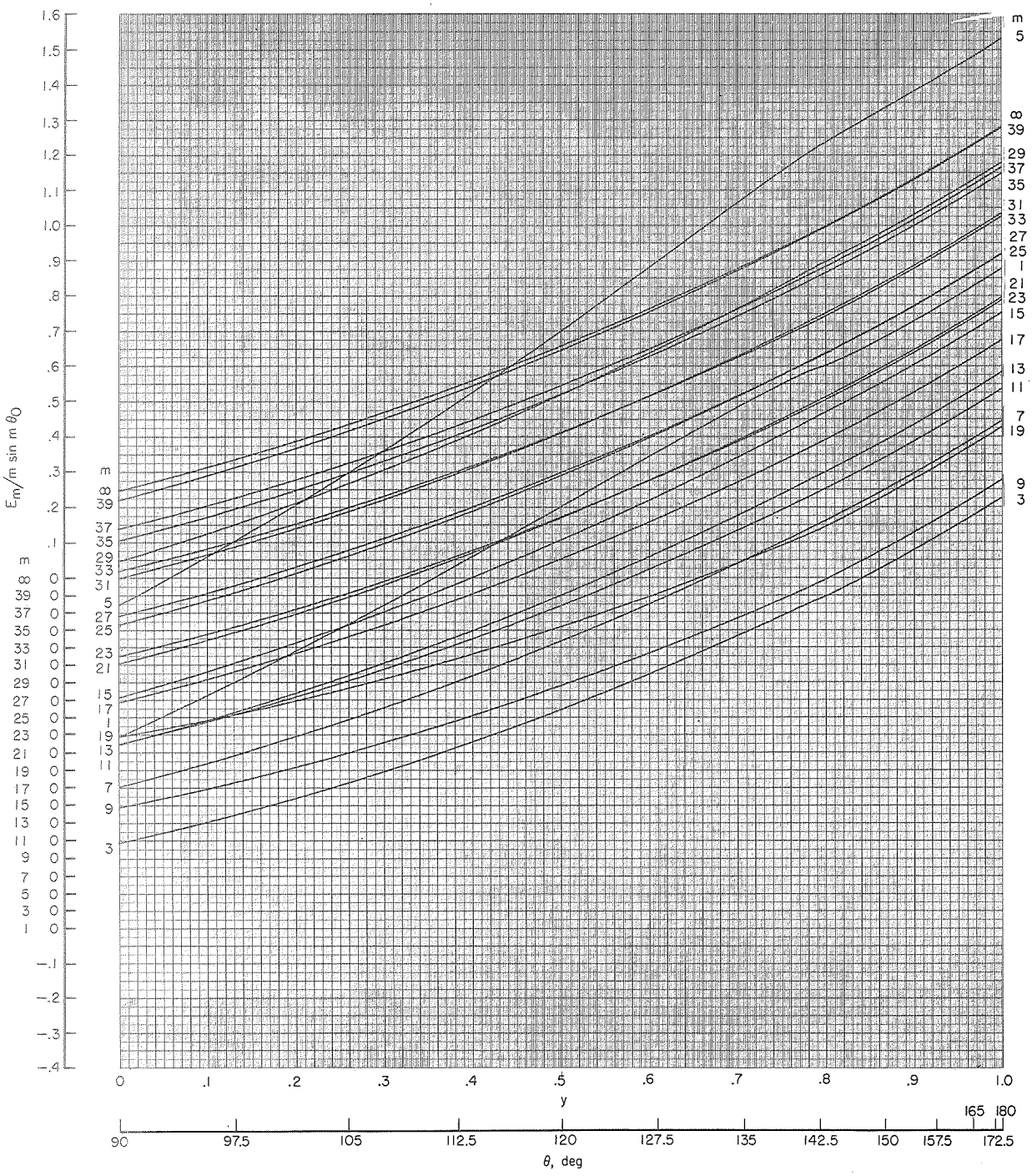

(h) $\theta_0 = 142.5^{\circ}$; $y_0 = 0.79335$.

Figure 9.- Continued.

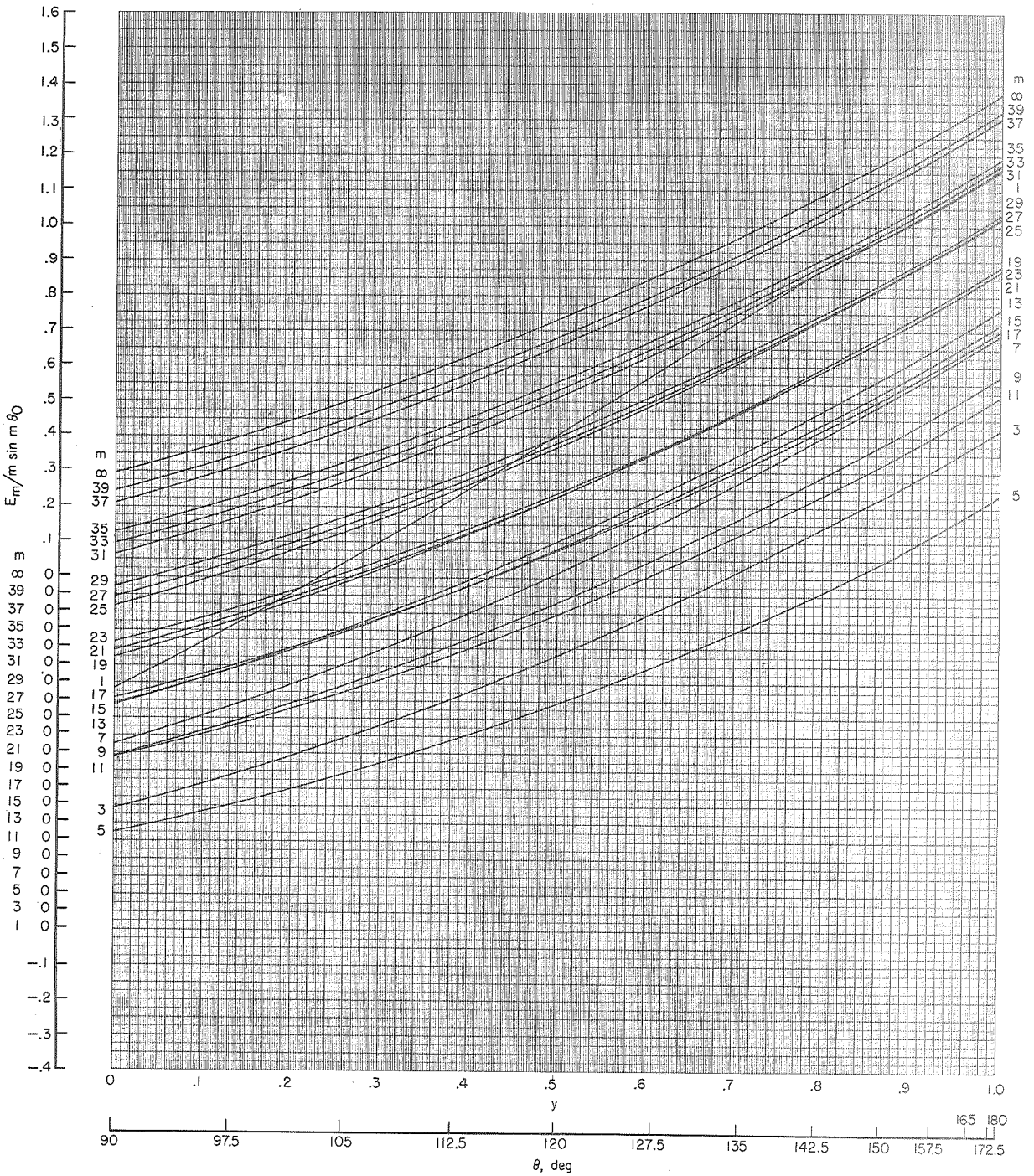

(i) $\theta_0 = 150^\circ$; $y_0 = 0.86603$.

Figure 9.- Continued.

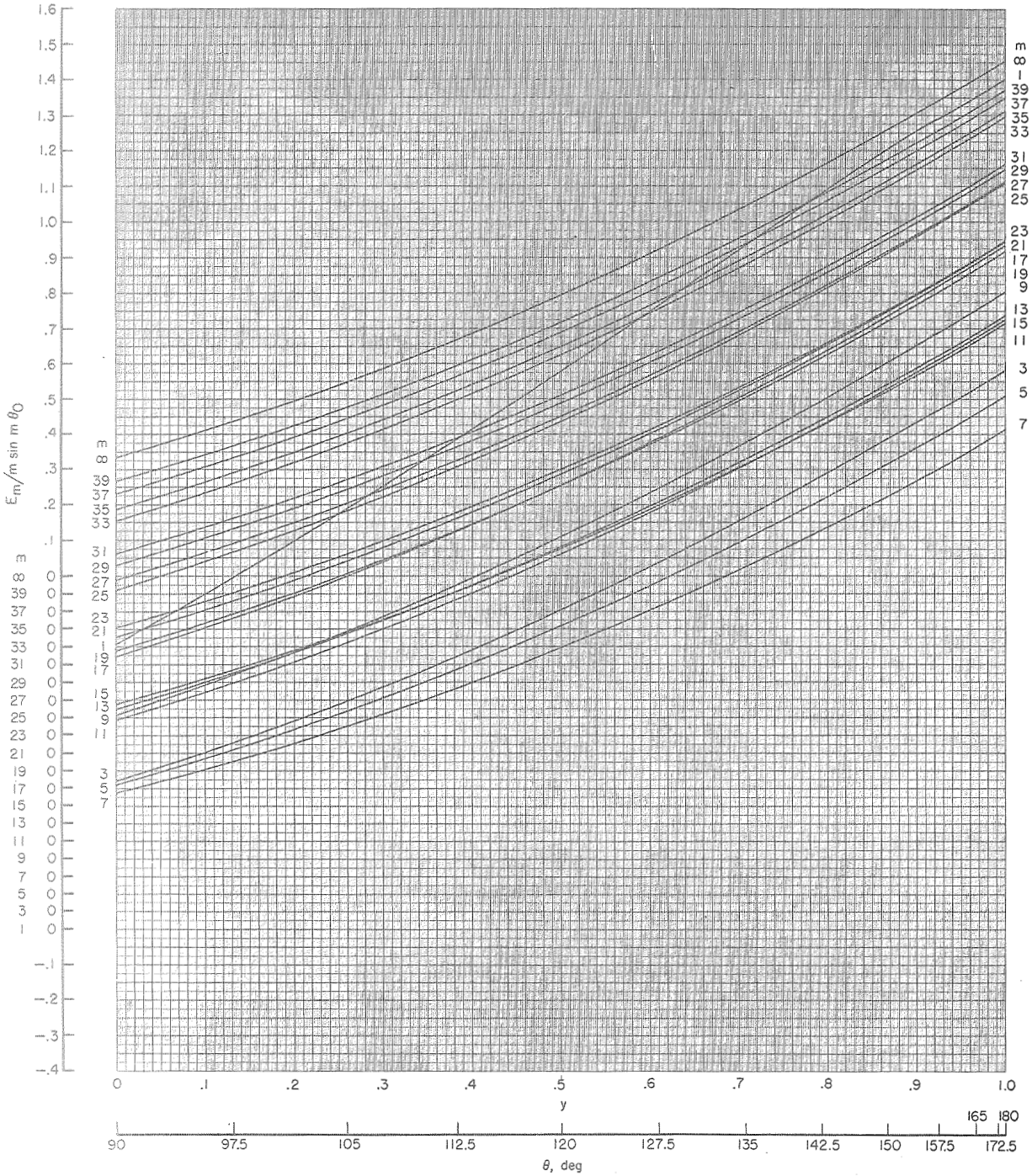

(j) $\theta_0 = 157.5^o$; $y_0 = 0.92388$.

Figure 9.- Continued.

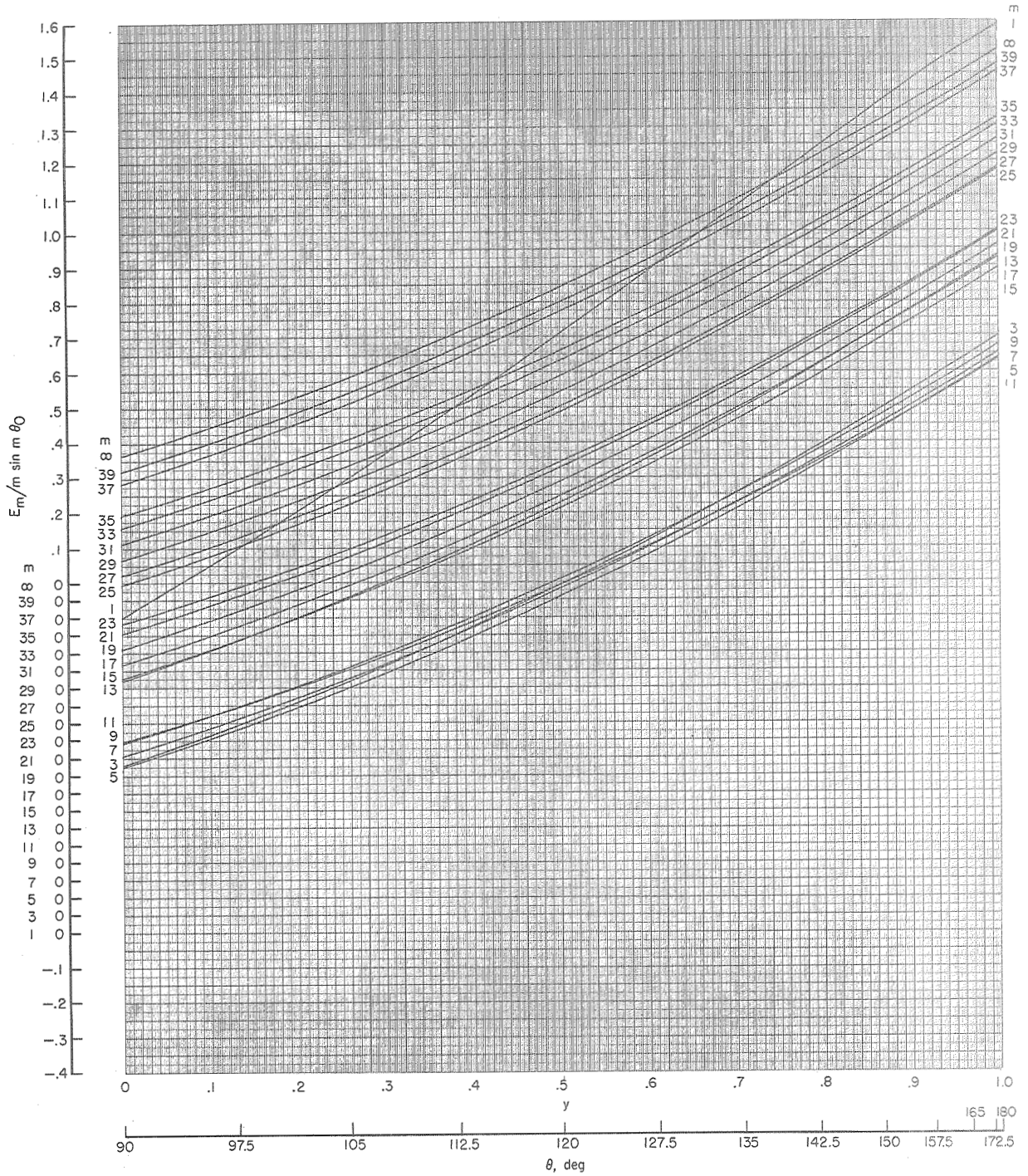

(k) $\theta_0 = 165^o$; $y_0 = 0.96593$.

Figure 9.- Continued.

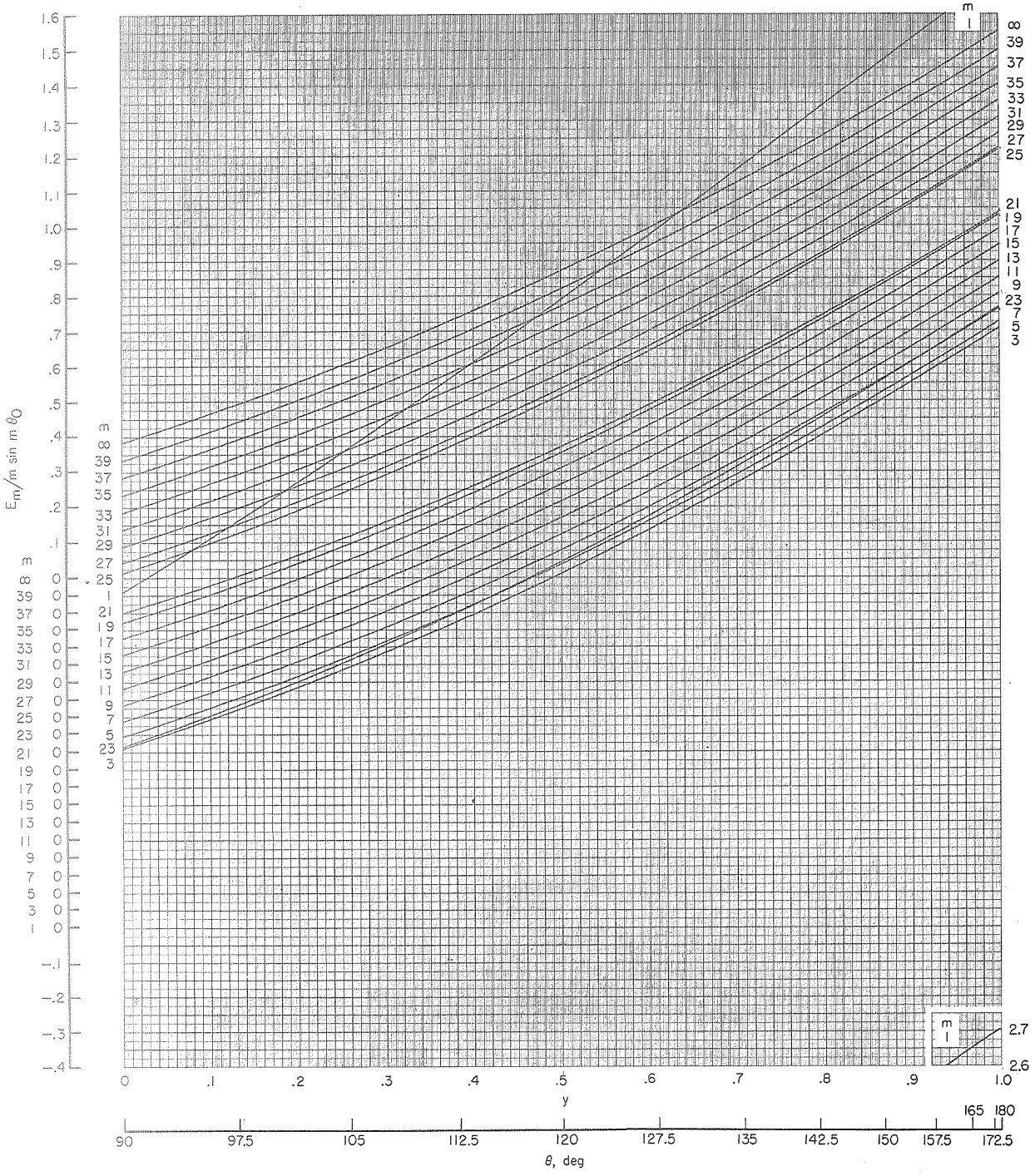

(*l*) $\theta_0 = 172.5^{\circ}$; $y_0 = 0.99144$.

Figure 9.- Concluded.

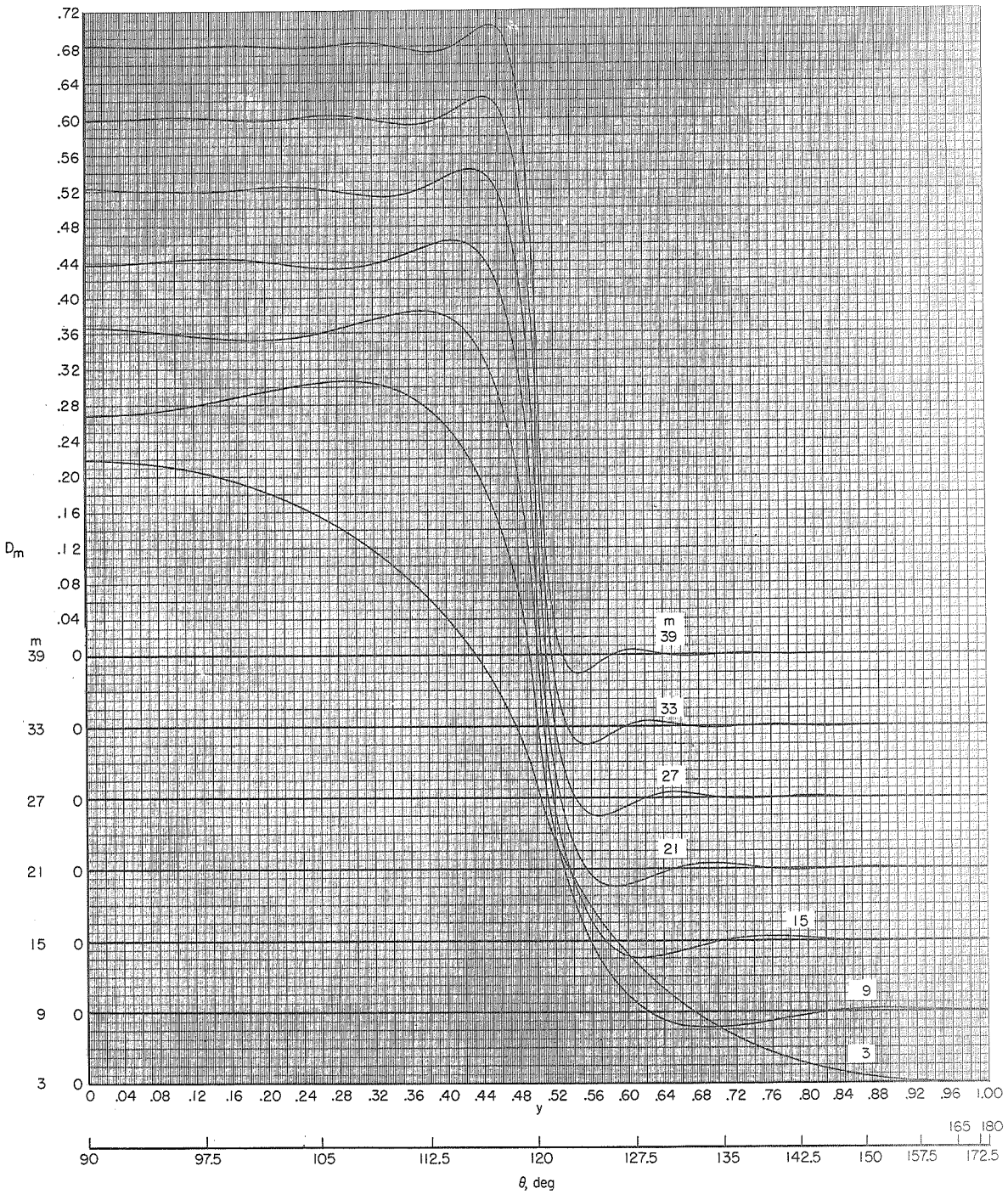

Figure 10.- D_m as a function of y for values of m which are odd multiples of 3 from 3 to 39 at $\theta_0 = 120^o$ and $y_0 = 0.5$.

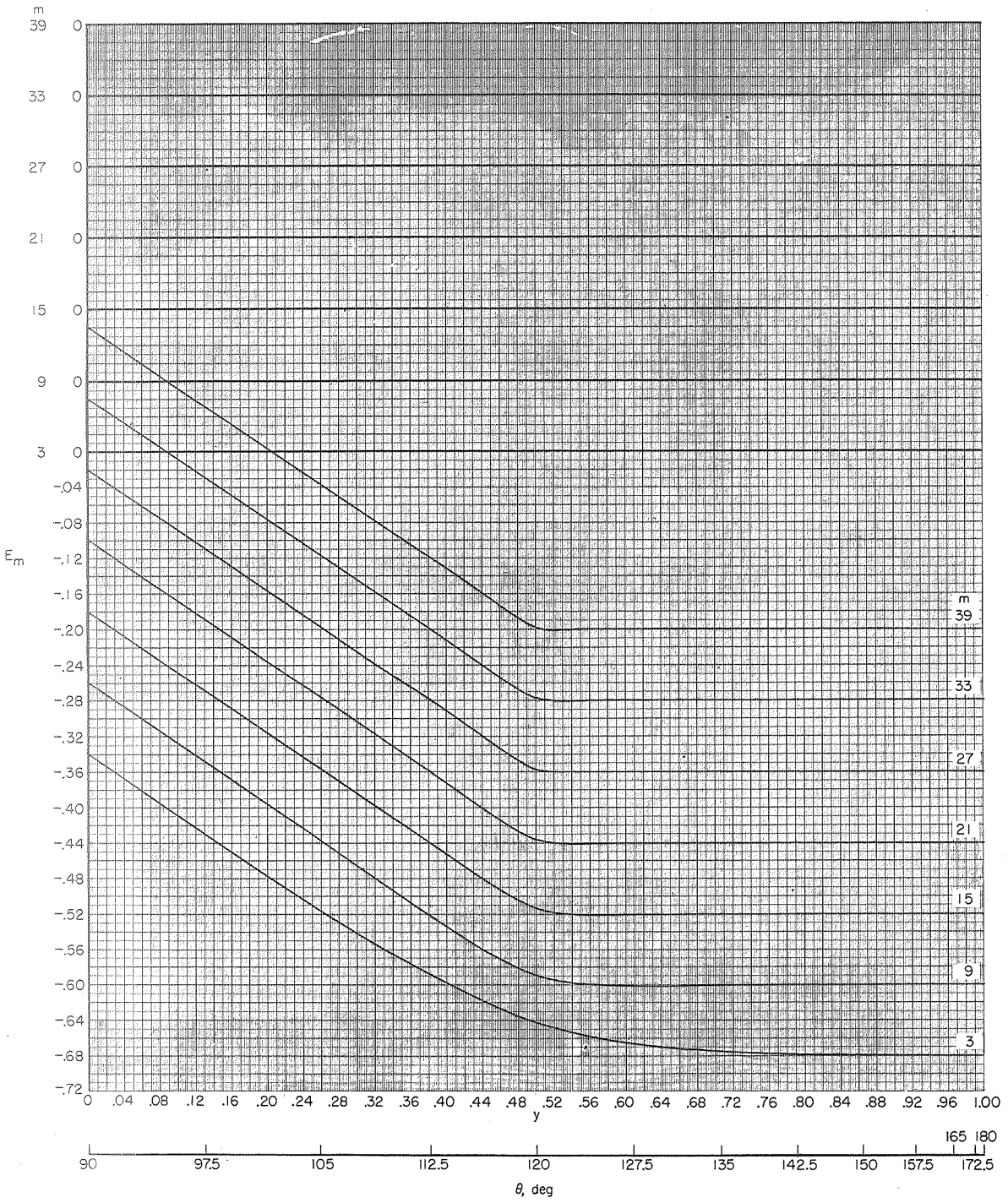

Figure 11.- E_m as a function of y for values of m which are odd multiples of 3 from 3 to 39 at $\theta_0 = 120^o$ and $y_0 = 0.5$.

NASA-Langley, 1971 —— 1 L-7666

"The aeronautical and space activities of the United States shall be conducted so as to contribute . . . to the expansion of human knowledge of phenomena in the atmosphere and space. The Administration shall provide for the widest practicable and appropriate dissemination of information concerning its activities and the results thereof."

—NATIONAL AERONAUTICS AND SPACE ACT OF 1958

NASA SCIENTIFIC AND TECHNICAL PUBLICATIONS

TECHNICAL REPORTS: Scientific and technical information considered important, complete, and a lasting contribution to existing knowledge.

TECHNICAL NOTES: Information less broad in scope but nevertheless of importance as a contribution to existing knowledge.

TECHNICAL MEMORANDUMS: Information receiving limited distribution because of preliminary data, security classification, or other reasons.

CONTRACTOR REPORTS: Scientific and technical information generated under a NASA contract or grant and considered an important contribution to existing knowledge.

TECHNICAL TRANSLATIONS: Information published in a foreign language considered to merit NASA distribution in English.

SPECIAL PUBLICATIONS: Information derived from or of value to NASA activities. Publications include conference proceedings, monographs, data compilations, handbooks, sourcebooks, and special bibliographies.

TECHNOLOGY UTILIZATION PUBLICATIONS: Information on technology used by NASA that may be of particular interest in commercial and other non-aerospace applications. Publications include Tech Briefs, Technology Utilization Reports and Technology Surveys.

Details on the availability of these publications may be obtained from:

SCIENTIFIC AND TECHNICAL INFORMATION OFFICE

NATIONAL AERONAUTICS AND SPACE ADMINISTRATION

Washington, D.C. 20546